Detonation of Mixtures of Nanometric or Flake Aluminum with Water

Geoffrey Chase

Department of Mechanical Engineering

McGill University

Montréal, Québec, Canada

August 11, 2021

A thesis submitted to McGill University in partial fulfillment of the requirements of the degree of

Master of Science in Mechanical Engineering

Abstract

The detonation of suspensions of nanometric and flake aluminum powders mixed with aqueous solutions of dilute hydrogen peroxide (H_2O_2) was experimentally investigated. The nano-Al powder was coated with 8–10 wt% Viton and had a nominal diameter of 91 ± 27 nm. The flake-Al powder was coated with 10 wt% trimethylolpropane trimethacrylate and had a surface area of 5.09 m^2/g. Detonation velocity and cylinder wall expansion tests were conducted in aluminum- and PVC-encased charges measured with shock pins and photonic Doppler velocimetry. Mixtures containing aqueous solutions of 10–20 wt% H_2O_2 detonated at 2.9–3.5 $km\,s^{-1}$, with variations in the detonation velocity attributed to variations in time-dependent density. Mixtures containing 10 wt% H_2O_2 solutions did not consistently detonate, indicating that porosity from hydrogen peroxide decomposition has a sensitizing effect. Mixtures containing only distilled water, 5 or 7.5 wt% H_2O_2 solutions, dilute ammonium nitrate solutions, glass microballoons, or micron-scale spherical aluminum powder failed to sustain detonation, but could potentially sustain detonation with optimization of the shot processing.

Abrégé

La détonation de suspensions de poudres d'aluminium nanométriques et en flocons mélangées à des solutions aqueuses de peroxyde d'hydrogène diluées (H_2O_2) a été étudié expérimentalement. La poudre d'aluminium nanométrique était recouverte de Viton avec une fraction massique de 8–10 % et les particules avaient un diamètre nominal de 91 ± 27 nm. La poudre d'aluminium en flocons était recouverte de triméthylolpropane triméthacrylate avec une fraction massique de 10 % et avait une surface de 5,09 m^2/g. Des essais de vitesse de détonation et d'expansion de paroi cylindriques ont été réalisés dans des charges enrobées d'aluminium et de PVC, mesurés à l'aide de pointes de choc et de vélocimétrie Doppler photonique. Les mélanges contenant des solutions aqueuses avec 10 à 20 % en fraction massique de H_2O_2 ont détoné à une vitesse de 2,9 à 3,5 $km\,s^{-1}$, les variations de vitesse de détonation étant attribuées aux variations de densité au cours du temps. Les mélanges contenant des solutions de H_2O_2 avec une fraction massique de 10 % n'ont pas détoné de manière systématique, ce qui indique que la porosité due à la décomposition du peroxyde d'hydrogène a un effet sensibilisateur. Les mélanges contenant

uniquement de l'eau distillée, des solutions de H_2O_2 avec 5 ou 7,5 % en fraction massique, des solutions diluées de nitrate d'ammonium, des microbilles de verre ou de la poudres micrométriques d'aluminium sphérique n'ont pas réussi à soutenir la détonation, mais pourraient potentiellement soutenir la détonation en optimisant le traitement de la charge.

Acknowledgements

I would like to thank, first and foremost, my supervisor Dr. David Frost. Without their support, unwavering patience, expert discussion, and careful review of my many manuscripts, I would not be where I am now. Secondly, I thank my unofficial co-supervisor Dr. Jason Loiseau, for venting and advice, and always being able to provide a second opinion.

I also must thank Dr. Jeffrey Bergthorson, Dr. Sam Goroshin, and the entire Alternative Fuels Laboratory group for all their support throughout my thesis, including, listening to and providing world-class feedback for my practice talks and presentations, their collaboration in research, and the many shared pitchers of blonde ale at Thomson House.

Many of the experiments described in this thesis would not have been possible without equipment and expertise provided by Keena Trowell, whose knowledge on aluminum-water reactions is unparalleled.

I would like to thank Rick Gilbeault (CanmetCERL) for their expert technical help towards this research, as well as the assistance and motivation of my most helpful undergraduate research assistants, Peter Wilk, Vishesh Pradeep, and Emeka Ngadi.

Finally, I need to acknowledge the help provided by my parents, family, and friends for their continued interest, support, and patience. This thesis is dedicated to my grandparents, Evelyn and Ernest Hawboldt, and Mary and Iwan Jürgens, my biggest supporters.

Contents

Acronyms **xii**

1 Introduction **1**

2 Literature Review **6**

2.1 Metal Combustion 7

2.2 Detonation Theory 13

2.3 Detonation Conditions 16

2.4 Metallized Explosives 17

2.5 Aluminum/Water Propellants 22

2.6 Aluminum/Water Detonation Reactions 23

3 Experimental **27**

3.1 Materials 29

3.2 Aluminum/Water-H_2O_2 Mixtures 32

3.3 Mixture Preparation 37

3.4 Charge Design 40

4 Results **45**

4.1 Nano-Al/Water-H_2O_2 Mixtures 45

4.1.1 Detonation of Nano-Al/Water-H_2O_2 45

4.2 Flake-Al Mixtures 49

4.2.1 Detonation of Flake-Al/Water-H_2O_2 49

4.2.2 Detonation of Other Flake-Al Mixtures 50

4.3 Micro-Al/Water-H_2O_2 Mixtures 51

5 Discussion **53**

6 Conclusions **60**

7 Future Work **63**

Appendix A Cheetah-Calculated Properties **83**

Appendix B Cheetah Input MATLAB Code **85**

Appendix C Analytic P-ν Behaviour from Wall Motion for Slab Geometry **88**

C.1 Pressure, P 89

C.2 Specific Volume of the Products, ν_p 89

List of Figures

2.1 Combustion of a 1 mm aluminum particle in 80 % H_2O/20 % CO_2 atmosphere demonstrating the lifted diffusion flame, molten aluminum droplet, and oxide cap. From [42]. 10

2.2 Detonation propagation through a long tube of aluminized NM explosive from Haskins et al. [3]. 14

2.3 ZND structure of 1D detonation. Adapted from [53]. 14

2.4 Phenomenology of 2D detonation flow. Adapted from Davis et al. [54]. . . . 15

2.5 Left: Pressure-time profiles of detonation of NM and NM-Al mixtures of varying particle size, from Kato et al. [78]. Right: Still frames showing detonation and delayed luminosity of 3 µm aluminum particles in NM indicating a reaction onset time of 15 µs, from [76]. The data on the left does not correspond to the experiments on the right. Direct comparison of the results of both experiments cannot be made, in this case, as experimental parameters such as Al mass fraction and charge diameter are dissimilar. . . . 21

3.1 TEM image of small-scale agglomerate of V-ALEX, courtesy of Keena Trowell. 30

3.2 SEM image of flake-Al particles in profile view. 31

3.3 Gas evolution for mixtures of U-ALEX and V-ALEX and water or diluted hydrogen peroxide solutions. Gas yield is normalized by the expected yield of the $2\,Al + 3\,H_2O \rightarrow Al_2O_3 + 3\,H_2$ reaction. 33

3.4 Production of gaseous O_2 products as a function of initial H_2O_2 concentration prior to explosive hydrogen production. The dashed lines show the expected amount of O_2 for different stoichiometries. 36

3.5 Density evolution of mixtures of flake-Al powder and solutions of 0, 5, 10, 15 and 20 wt% H_2O_2 in water, with TMD of 1.401/1.415/1.432/ 1.450/1.468 $g\,cm^{-3}$, respectively. 37

3.6 Prepared V-ALEX/water-H_2O_2 mixture. 38

3.7 Flake-Al mixture before (left) and after (right) acoustic mixing. 39

3.8 Charge geometry of shots #1–7. 41

3.9 Assembled charge used in shots #1–7. 42

3.10 Charge geometry of shots #8–13 (left) and #14–22 (right). 43

3.11 Charges used in shots #8–13 (left) and #14–22 (right). 44

4.1 Recovered case fragments from trials containing mixtures of nano-Al. 47

4.2 PDV velocity histories for 0 and 5 wt% H_2O_2 V-ALEX experiments that failed before the end of the charge. 48

4.3 PDV velocity histories for 10 and 15 wt% H_2O_2 V-ALEX experiments that detonated until the end of the charge. 48

4.4 Shock velocity variation along length of detonated flake-Al shots. 51

5.1 Comparison of experimental results of nano-Al/water-H_2O_2 detonation and results calculated by Cheetah 2.0. 54

5.2 Experimentally measured P-ν evolution of the nano-Al system products compared to the predicted JWL-fit product isentropes by Cheetah. 56

5.3 Comparison of experimental results of flake-Al/water-H_2O_2 detonation and results calculated by Cheetah 2.0. 57

List of Tables

2.1 Nitromethane detonation with added aluminum from Cheetah 2.0. 18

2.2 Specific heat of formation of aluminum oxides [98]. 24

4.1 Summary of detonation experiments. Weights are tabulated by percent mass in the aqueous solution. Densities are reported as measured. 46

A.1 Al/Water-10 wt% H_2O_2 detonation properties and JWL coefficients from Cheetah 2.0, BKWC library. Initial density $\rho_0 = 0.95\,\mathrm{g/cm^3}$. 84

Acronyms

AN	Ammonium nitrate, an explosive
ANFO	Ammonium nitrate/fuel oil, an explosive mixture
BKW	Becker-Kistiakowsky-Wilson
C-4	Composition C-4, an explosive
CJ	Chapman-Jouguet
CRZ	Chemical reaction zone
EOS	Equation of state
GMB	Glass microballoon
HE	High explosive
HMX	Cyclotetramethylenetetranitramine, an explosive
HzMN/Hz	Hydrazinium mononitrate/hydrazine, an explosive
ID/OD	Inner/Outer diameter
JWL	Jones-Wilkins-Lee
MW	Molecular weight

NM	Nitromethane, an explosive
PDV	Photonic Doppler velocimetry
PETN	Pentaerythritol tetranitrate, an explosive
PVC	Polyvinyl chloride
RDX	Cyclotrimethylenetrinitramine, an explosive
TATP	Triacetone triperoxide, an explosive
TMD	Theoretical maximum density
TNT	Trinitrotoluene, an explosive
TRIM	Trimethylolpropane trimethacrylate
U-ALEX	Uncoated nano-aluminum
V-ALEX	Viton-coated nano-aluminum
VoD	Velocity of detonation
ZND	Zel'dovich-von Neumann-Döring

Chapter 1

Introduction

Aluminum powder is a common additive to explosive and propellant formulations to enhance energy density. Consequently, the influence of aluminization on explosive performance has been well-studied. Owing to the difficulties with direct diagnostics of the optically-thick detonating media and violent nature of the condensed phase detonation, most conclusions regarding aluminum reaction dynamics have been obtained from the observation of the effect of the inclusion of aluminum particles of varying size, mass fraction, and morphology on the detonation performance parameters (e.g., detonation velocity, pressure, heat release) of the explosive.

Three distinct types of aluminized explosive are considered: 1) conventional monomolecular high explosives (HEs) with a high detonation velocity (VoD) (e.g., TNT, RDX, PETN), 2) low VoD, strongly oxidizing explosives (e.g., ammonium nitrate,

ammonium perchlorate), and 3) detonable mixtures of strong oxidizers and fuels (e.g., Sprengel explosives).

In the first case of conventional monomolecular explosives, it is generally understood that when aluminum is added to these HEs, the aluminum is practically inert in the detonation reaction zone [1–4]. This engineering simplification arises from the decrease in detonation properties observed both with inclusions of aluminum and with chemically inert diluents such as lithium fluoride.

However, in these explosives, the aluminum is not truly inert. The endothermicity of aluminum reactions occurring promptly within the chemical reaction zone (CRZ) of HEs was noted in early work by Cook et al. [5]. More recently, investigations of the deuterium isotope effect by Tappan et al. have shown a significant fraction of aluminum reacting in the detonation CRZ of HMX and HzMN/Hz [6]. One notable example exists where the inclusion of nanometric aluminum in TNT has been shown to provide prompt exothermicity and increase the bulk VoD and heat of detonation [7].

Additionally, in these explosives, evidence of early post-detonation reactivity of aluminum has been documented. Reactivity of aluminum early in product expansion has been indicated in experiments studying confiner acceleration by aluminized explosives [8,9] and the strength of the near-field blast wave from aluminized nitromethane (NM) [10].

When aluminum particles are added to the second class of explosives noted above, i.e., strong oxidizers with long reaction zones, the aluminum has been shown to react with the

CRZ on a microsecond time scale. Powdered aluminum, in a size range from a few to tens of microns, can easily detonate with ammonium nitrate (AN) [11], and ammonium perchlorate [12]. In these formulations, which are difficult (but not impossible) to detonate without aluminization, aluminum powders added as a fuel component enhance the detonability and can react in a sufficiently fast timescale to enhance the bulk detonation properties [11, 12]. In the first half of the 20^{th} century these so-called ammonals were a mainstream military and industrial explosive.

The third type of explosives, comprised of mixtures of non-detonable fuel and oxidizer components, is the subject of this thesis. The aluminum fuel and $\sim$10 wt% hydrogen peroxide in water oxidizer are each not considered capable of sustaining detonation on their own. The metal-oxidizer system examined in this work presents a binary model for investigating timescales of aluminum reaction with water in extreme conditions. The participation of the micron-scale flake aluminum used in this work in energetically supporting a detonation, faster than previously thought possible with a weak oxidizer such as water, is relevant to understanding the role of aluminum reaction in the detonation of conventional, composite explosives which produce water as a primary product of combustion. Moreover, many strong oxidizers mixed with aluminum present a sensitivity hazard for large-scale tests for laboratory investigation. The sensitivity to electrostatic discharge, impact, and shock of the aluminum-water system has been characterised in a previous study [13] and shown to be insensitive.

From the perspective of thermophysical uncertainty in aluminum combustion in the

extreme conditions of the detonation environment (as described in Section 2.4), a more direct measurement of aluminum reaction mechanisms and timescales in the detonation front is required. It is impossible to extrapolate results of burning rate experiments performed at moderate conditions [14] to when aluminum particles burn in extreme pressure and temperature environments.

In this study, the detonability of both nano- and conventional flake-Al mixtures with water-based oxidizing solutions in cylindrical charges was considered. In nano-Al tests, photonic Doppler velocimetry (PDV) was used to measure cylinder expansion velocity. In flake-Al tests, shock pin diagnostics provided detonation velocity data. This work presents the first evidence of detonation in commercially available flake aluminum powder-water binary mixtures.

Although nanoscale spherical particles have the potential for enhanced reactivity due to their large surface area, spherical nanopowders have several disadvantages when compared to flake powder for large-scale tests of reactions with water; nano-Al powders are more expensive, suffer from a larger fraction of a naturally-forming inert oxide, and have a greater potential to react explosively with water than comparably larger aluminum particles. Lower cost, increased stability, and high aluminum content are favourable attributes of the flake-based system.

The current research concerning Al/water-H_2O_2 detonation is limited in dataset and scope, and does not attempt to elucidate the effect of mixture components on detonability.

Past research by Schmitt et al. [15] investigated only formulations containing nanometric aluminum powders mixed with stoichiometric 10 wt% dilute hydrogen peroxide in water. In total, only 5 total detonation tests were completed (3 trials detonated, 2 trials failed to sustain detonation). The objective of this thesis is to investigate experimentally the existence of a detonation mode of propagation for the aluminum-water system, and shed light on the sensitizing effects of hydrogen peroxide and particle morphology for systems primarily composed of nanometric or flake aluminum particles mixed with water. To accomplish this, mixtures of varying peroxide concentration and oxidizer formulations were tested.

The content of this thesis will be structured as follows. The second chapter provides a review of the literature of aluminum combustion in a variety of combustion regimes, from quiescent single particle combustion to the combustion of particles in the detonation environment. The third chapter describes an overview of the experimental techniques used to evaluate the detonation behaviour of the aluminum-water system, including a description of materials used, reactivity properties of mixtures of aluminum and aqueous hydrogen peroxide, techniques for bulk mixture preparation, and design of explosive charges used. The following chapters provide results of the field experiments, and discussion of how the results obtained contribute to our understanding of the nature of aluminum-water detonation. Finally, conclusions based on the work performed and recommended continuations for future work are presented.

Chapter 2

Literature Review

The purpose of this chapter is to provide an overview of the features of aluminum particle combustion in systems ranging from relatively slow flows to the extreme conditions attained by the detonation of a HE. Although our understanding of metal particle combustion is rudimentary in comparison to the combustion of gaseous fuels, considerable information is available regarding the ignition and combustion of aluminum particles in quiescent conditions at atmospheric pressures. In contrast, virtually nothing is known about how aluminum particles burn in the extreme conditions behind a detonation wave in a condensed explosive, with pressures on the order of 10 GPa, temperatures in the thousands of Kelvin, and relative flow between phases on the order of $1\,\mathrm{km\,s^{-1}}$.

2.1 Metal Combustion

In all applications of metal flames, ranging from the mitigation of accidental metal dust explosions to the use of metal powders as a renewable fuel, there remains a fundamental interest in the characteristics of the metal combustion. Historically, experiments studying metal powder combustion include the addition of metal powders to the combustion products of hydrocarbon burners or in air in a variety of configurations, including freely propagating dispersed powder flames [16], flames propagating in tubes [17], spherically expanding isobaric flames [18], flames in constant volume combustion bombs [19, 20], and burner-type experiments such as Bunsen flames [21–23], flat flames [21], and counterflow flames [24, 25]. Metal combustion is also studied in induction-type experiments utilizing shock tubes [26–28] and ovens [29, 30]. The duration of luminosity of the burning metal particles, which is strongly correlated with high temperatures and therefore reaction, has been used as an indication of particle ignition delay and reaction time [21, 26, 27]. In stationary flame front burner-type experiments, particle image velocimetry may be conveniently used in heterogeneous flames to infer flame speed [24]. In all optically accessible configurations, reaction characteristics may be determined by recording the emission or absorption of light by the bulk flame, for example, by optical pyrometry [23, 31–33] or absorption spectrometry [23, 28, 31], respectively. Particle ignition delay, burning rate, and reaction regime depend on pressure, temperature, and type of oxidizer. Unfortunately, due to the extreme conditions of condensed phase detonations, it

is more difficult to identify combustion regimes by applying spectroscopic techniques to the detonation products.

According to the thermal ignition theory derived by Frank-Kamenetskii and Vulis [34–36], two regimes are identified to describe the combustion of metal flames: kinetic-, or diffusion-limited regimes. The overall effective reaction rate $\dot{\omega}_{\text{eff}}$ for a particle is dependent on the competition between the rates of chemical kinetics and oxidizer diffusion: $\dot{\omega}_{\text{eff}} \propto k\beta/(k+\beta)$, where k is the Arrhenius kinetic rate and β is the mass diffusion coefficient between a particle and the oxidizing gas. In the kinetic-limited regime, the oxidizer diffuses at a rate much higher than the chemical kinetic rate, exhibiting an exponential dependence on particle temperature, lower than the stoichiometric flame temperature. The kinetic-limited regime is also known as the small particle regime, as β is inversely proportional to particle diameter. In contrast, the diffusion-limited regime is limited by the diffusion of oxidizer to the reaction surface, and the high rate of reaction ensures that the reaction surface burns near the stoichiometric flame temperature. Lifted flames may occur in diffusion-limited regimes of combustion where the stoichiometric flame temperature is greater that the boiling point of the metal [37], as is the case with aluminum.

In single-particle ignition, the relatively cool particle initially reacts in the kinetic-limited regime. As more energy is released as heat, if the heat generation rate is greater than the heat loss rate, the particle 'ignites' and transitions to the diffusion-limited regime. Conversely, larger particles burning in the diffusion-limited regime will lose mass and transition to the

kinetic regime, as particle 'extinction' occurs, before continuing to burn in the kinetic regime. The transition between the kinetic- and diffusion-limited regimes is analogous to Semenov reactor ignition theory [38]. Smaller particles initially below the critical size will burn entirely in the kinetic regime. The critical particle diameter of aluminum for ignition is dependent on a variety of factors including flow conditions, fuel and oxidizer properties, as well as reaction specific heat release and activation energy. To gain an understanding of particle scale in the transition between combustion regimes for aluminum particles, a transitional regime diameter can be estimated as 4.4 µm based on numerical values of gas and solid-fuel parameters [39], and shown experimentally to occur at approximately 10 µm in size in shock tube experiments [31].

Particle burn time is a consistently studied metric related to particle reaction rate. An idealised basic mass balance[1] of a diffusion-limited burning particle yields a burn time proportional to the square of the particle diameter $\tau_B \propto d^2$ [35, 37] for particles in quiescent conditions with a constant Sherwood number[2]. Experimentally, particles exhibit a reduced exponent $\tau_B \propto d^{n<2}$ because of non-idealities such as oxide accumulation on the particle surface inhibiting diffusion. A multi-study review by Beckstead [14] of experimental measurements of burning time for 15–750 µm Al particles found an overall correlation of $\tau_B \propto d^{1.8}$, normalized slightly by oxidizer concentrations, pressure and initial temperature.

[1] $\tau_{B,\text{diffusion}} \approx m/\dot{m} \propto d^3/d^2\beta C_\infty = d^2/\text{Sh}DC_\infty$, $\tau_{B,\text{kinetic}} \approx m/\dot{m} \propto d^3/d^2kC_\infty = d/kC_\infty$

[2] The Sherwood number is the ratio of convective and diffusive mass transport. Empirical correlations for spheres are of the form $\text{Sh} = 2 + C\text{Re}^n\text{Sc}^m$ [40]. In quiescent conditions with little relative flow, $\text{Re} = 0$ and $\text{Sh} = 2$.

As combustion theory indicates the transition to kinetic-limited combustion at smaller diameters, a similar analysis[1] for particle burn time for smaller particles reacting in the kinetic regime can show the linear diameter correlation $\tau_B \propto d^1$ [35, 37], which also varies with ambient experimental conditions, such as the Arrhenius dependence on gas temperature, and pressure [28, 31], and which also follows a reduced exponent $\tau_B \propto d^{n<1}$ when observed experimentally [31, 41]. The usefulness of the d^n scaling is sometimes questioned but still provides a rudimentary indication of combustion regime. In general, a burn time exponent may not be completely indicative of the combustion regime and should be used in conjunction with other diagnostics. The transition from the d^2 to d^1 scaling can be observed in the radius-time profiles in the single-particle thermophysical model of Soo et al. [39].

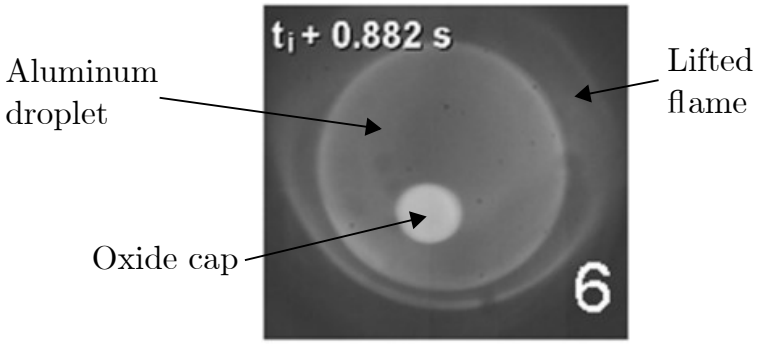

Figure 2.1: Combustion of a 1 mm aluminum particle in 80 % H_2O/20 % CO_2 atmosphere demonstrating the lifted diffusion flame, molten aluminum droplet, and oxide cap. From [42].

In the combustion of particle clouds, a collective heating effect is observed where particle reaction rate is accelerated by heat release from neighbouring particles. Oxidizer

concentration may no longer be considered infinite and the mixture's fuel and oxidizer fractions are consequently of importance. Soo et al. [36, 39] used a thermophysical framework to investigate and compare the combustion of single particles, clouds, and agglomerates. The combustion characteristics of the cloud model range from when applied to fuel-dilute clouds, approximating results obtained by considering only the single particle, to denser clouds, where a nonobvious dependence of combustion time on fuel mass concentration and particle size was found. In general, the collective effect accelerates combustion when compared to single particle theory, decreasing particle reaction time and lowering the required temperature to induce reaction in non-adiabatic particle clouds. Clouds of particles may support reaction through the collective effect even in the kinetic regime where individual particle ignition will not occur. Additionally, it was found that particle agglomeration presents an often overlooked, double-edged effect on combustion characteristics depending on multiple parameters including the degree of agglomeration and agglomerate and particle size. Julien et al. [43] seeded methane flames with 6.5 µm aluminum particles and observed that below a critical concentration, the aluminum acted as an inert diluent to the methane flame and resulted in a deficit in the methane flame speed. Above the critical concentration, the aluminum flame front coupled to the hydrocarbon flame and resulted in a plateau of burning velocity due to heat transfer from the slowly-reacting, but high aluminum flame temperature into the quickly-reacting methane flame front.

Most experimental studies of metal combustion in air have relatively low air flow velocity over the metal particle. In non-quiescent high-speed flow, such as the conditions achieved in the post-detonation flow of HEs, convective effects leading to liquid film stripping of the molten metal droplet may occur [33, 35]. High-speed flow promotes increased heat and mass diffusion by convection and promotes the reaction to transition to the kinetic regime. Tanguay et al. [41] experimentally studied the combustion of aluminum and magnesium powders in the products of gaseous detonations and utilised emission spectra and luminosity to measure particle temperature, burn time, and ignition delay. It was concluded that particles (of sizes 5–100 µm) burned in the kinetic regime, evidenced by a burn time $\tau_B \propto d^{0.5}$ and emission spectroscopy temperature measurements. A model developed for reaction delay prediction based on an ignition criterion, such as the particle reaching the melting temperature of aluminum or its oxide, did not match experimental results. Tanguay also concluded that larger particles than those that were used in the study would be required to show evidence of the film stripping effect.

Experiments demonstrating reaction-induced stripping of bulk metal in high speed flow were performed by Tanguay et al. [41] investigating the reaction of millimetric metal rods placed in shock-accelerated (Mach 5–9) oxygen. Control experiments performed with nitrogen showed no ablation, indicating that a reaction occurred on the metal surface. 'Burning bullet' experiments by Higgins et al. [44] and Batchelor et al. [45] demonstrated the shock-induced surface combustion of supersonic millimetric metal spheres in high

pressure oxygen, with limited datasets. Further experiments were conducted using titanium spheres by Devito et al. [46], who developed a model to predict critical ignition parameters of velocity and pressure and incorporated spectroscopic techniques.

2.2 Detonation Theory

A detonation wave is a supersonic combustion wave. In the detonation wave, a compressive shock wave initiates the combustion reaction in an explosive. The combustion reaction releases chemical energy which, in turn, supports the shock wave [47]. Figure 2.2 illustrates a typical detonation of a long cylindrical explosive charge which shows the detonation wave traveling from top to bottom and the expanding products flowing outwards.

A one-dimensional treatment of the detonation wave structure was developed during the Second World War independently by Zel'dovich [48], von Neumann [49], and Döring [50], known as the ZND structure. In this treatment, an infinitesimal leading shock wave of velocity D initiates a CRZ of finite width. As chemical energy is deposited into the supersonic flow, pressure decreases from a 'von Neumann spike' and the flow decelerates (in the frame of the leading shock wave) to a sonic velocity at the end of the reaction zone, known as the the Chapman-Jouguet (CJ) state [47, 51, 52]. After the CJ state, the flow expands in a Taylor rarefaction wave to a constant state. The ZND structure is shown in Figure 2.3.

The sonic surface corresponds to a barrier for wave propagation from products toward the shock front, so that no information can be communicated from behind this point upstream.

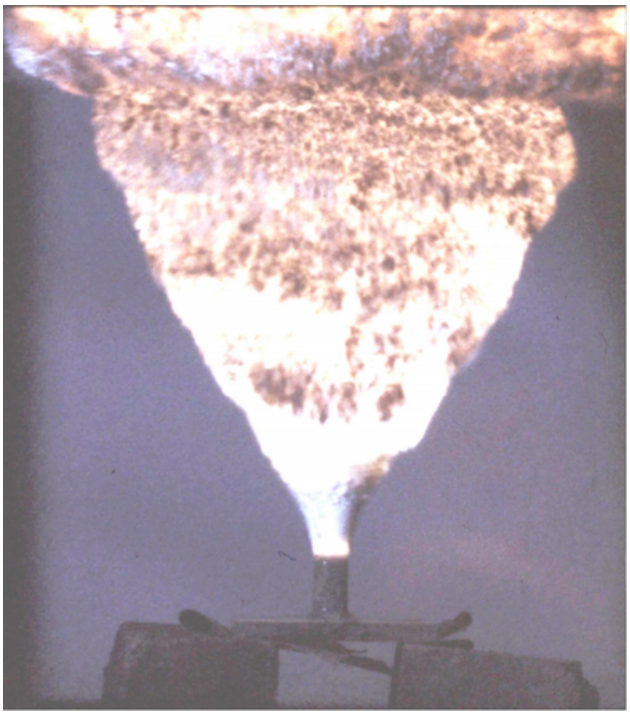

Figure 2.2: Detonation propagation through a long tube of aluminized NM explosive from Haskins et al. [3].

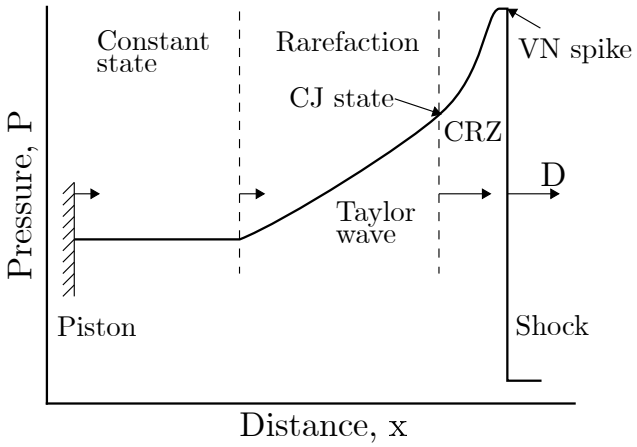

Figure 2.3: ZND structure of 1D detonation. Adapted from [53].

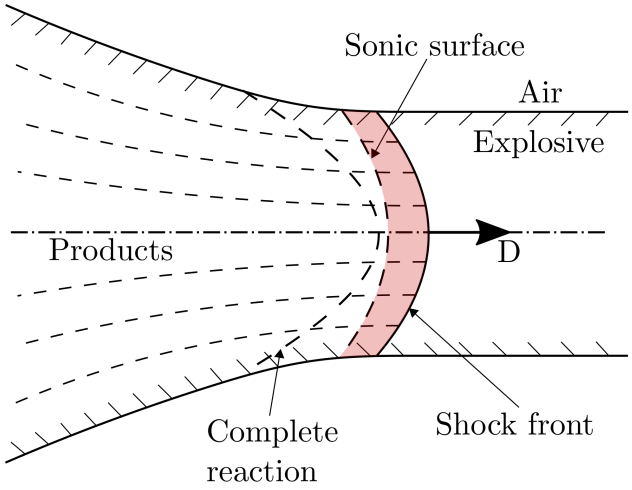

Figure 2.4: Phenomenology of 2D detonation flow. Adapted from Davis et al. [54].

Any reactions that occur after this point will not influence the detonation wave. In ideal 1D explosives, the reactants just reach sonic velocity as the reaction reaches completion. In non-ideal explosives (explosives that cannot be treated as one-dimensional), such as the heavily aluminized explosive studied in this work, energy losses due to radial expansion allow the detonation products to continue releasing energy well past the sonic surface, often termed as an *eigenvalue detonation* [47]. Figure 2.4 illustrates features of the non-ideal detonation propagating through an explosive material of finite diameter at velocity D, including shock front curvature and reaction extended past the sonic plane.

Between this sonic plane and the shock front is the so-called detonation reaction zone. In this zone, temperatures are $\sim$3000 K, and condensed phase explosive pressures are in the tens of GPa [55]. Additionally, this wave is travelling through the explosive at kilometers per second, and this reaction zone is less than a millimeter thick, so the reactions that support

the detonation wave are occurring in microseconds.

A conventional explosive's energy is released in this reaction zone, followed by a long expansion zone. When aluminum particles are added to the explosive, they are historically assumed not to react when passing through the reaction zone, absorbing energy, then continue and react later with oxidizers in the combustion products or surrounding air on timescales of milliseconds.

2.3 Detonation Conditions

The detonation pressures obtained in the CRZ of condensed phase detonations are much higher than those found in gaseous phase detonations, and on the order of 10–30 GPa for condensed phase [55] compared with 10 MPa for gas phase [47, 55]. The detonation pressures in condensed explosives are therefore significantly higher than the compressive strength of metal powders embedded in the detonating material and may lead to particle deformation [56] and destruction of the integrity of the aluminum oxide shell. Additionally, highly supercritical water in the detonation products will also likely dissolve the oxide coating, rendering it permeable to water [57–59].

Cheetah is a thermochemical equilibrium solver designed to solve the conservation equations of mass, momentum, and energy across upstream and downstream conditions, coupled with an equation of state (EOS) (e.g., the Becker-Kistiakowsky-Wilson (BKW) [60] or Jones-Wilkins-Lee (JWL) [61] EOSs for condensed phase explosives), as

well as chemical potentials at the CJ state using Gibbs energy minimization [62]. Cheetah can be used to provide a quick estimation of fundamental explosive properties such as detonation velocity and CJ pressure with the assumption that equilibrium conditions are attained at the downstream CJ plane. The theoretical performance of explosives determined using the Cheetah code may be compared to experimental results, keeping in mind the limitations of the application of 1D detonation theory. Finite rate chemistry and Wood-Kirkwood diameter effects (i.e., the dependence of detonation velocity on the curvature of the detonation front) may also be evaluated for some explosives [63].

The evaluation of CJ parameters by Cheetah 2.0 for a NM detonation with 0–30 wt% added aluminum is shown in Table 2.1, using the BKWC EOS library. The amount of aluminum which fully reacts in the 1D system has been varied from 0–100 % to illustrate the effect of the degree of aluminum reaction on detonation parameters. Non-idealities, such as an oxide fraction which may be significant for small particles, or a decreased density due to particle agglomeration, mixing conditions, and gas generation, have been neglected for clarity. The prompt reaction of aluminum increases the CJ state detonation pressure and temperature.

2.4 Metallized Explosives

Heterogeneities, such as solid or hollow particles, introduced into explosives often provide a mechanism of sensitization where detonation would otherwise fail [64]. Work by

	NM	NM + fully reacting Al	NM + 50 % reacting Al	NM + inert Al
Mass fraction NM/Al/inert Al	100/0/0	70/30/0	70/15/15	70/0/30
Initial density ρ_0, $\mathrm{g\,cm^{-3}}$	1.160	1.399	1.399	1.399
Pressure P_{CJ}, GPa	11.89	12.26	11.83	9.35
CJ Density ρ_{CJ}, $\mathrm{g\,cm^{-3}}$	1.591	1.877	1.880	1.792
Energy E, $\mathrm{kJ\,cm^{-3}}$ expl.	1.61	1.56	1.51	1.02
Temperature T, K	3669	5190	4075	2752
Shock velocity D_{CJ}, $\mathrm{mm\,\mu s^{-1}}$	6.149	5.868	5.753	5.525
Particle velocity u_{CJ}, $\mathrm{mm\,\mu s^{-1}}$	1.667	1.493	1.470	1.209
Speed of sound c_{CJ}, $\mathrm{mm\,\mu s^{-1}}$	4.483	4.374	4.283	4.316
Gamma γ	2.690	2.929	2.913	3.568
Total energy of det. E_{tot}, $\mathrm{kJ\,cm^{-3}}$	-5.637	-12.407	-8.045	-4.913

Table 2.1: Nitromethane detonation with added aluminum from Cheetah 2.0.

Engelke [65, 66] found that the addition of chemically inert glass beads into NM lead to a significant reduction in critical charge diameter (i.e., the minimum charge diameter for which a detonation is self-sustained). Localised energy concentrations called 'hot spots', are formed by shock wave interactions with entrained heterogeneities, such as voids within the mesostructure of a crystalline explosive, or added solid powders [67, 68]. Several mechanisms for the formation of hot spots have been proposed, such as pore collapse, jetting, and shock collision around a high-impedance obstacle [69, 70], but the relative importance of the mechanisms remains unclear. Hotspot effects may be studied experimentally [65, 66, 71], or by using 2D and 3D mesoscale models [56, 67, 72, 73].

Explosives with microscopic heterogeneities may still be ideal explosives. Bulk explosives which exhibit full decomposition over a short (microns for several explosives) lengthscale before expansion of the products after the detonation sonic surface are

considered 'ideal'. Conversely, a 'non-ideal' explosive is characterized by a reaction zone where a significant fraction of unburned explosive extends well into the product expansion [74], or contains additives such as large aluminum particles which continue to burn within the product gases. Binary explosives, which are comprised of a heterogeneous, and potentially multiphase mixture of fuel and oxidiser [55], are an example of non-ideal explosives which, rather than being a monomolecular explosive undergoing thermal decomposition, require direct contact between the fuel and oxidiser for reaction. A commonly used non-ideal heterogeneous explosive is the binary mixture of AN prills (pellets) in fuel oil (ANFO). Characteristic of non-ideal explosives, ANFO exhibits a reaction zone length measured in centimeters, a steep detonation velocity vs. reciprocal diameter curve, and a large critical diameter [75, 76].

Aluminum, an energy-dense material typically in the form of nano- to micron-scale spherical or flake powders, is a common additive to explosive compositions to enhance the explosive effects. In general, the specific energy of HEs is 5–6 $\mathrm{MJ\,kg^{-1}}$, whereas the complete oxidation of aluminum has a specific energy of 31 MJ/kg-Al, or 16 $\mathrm{MJ\,kg^{-1}}$ with oxidizer. Explosives used during the Second World War with compositions using aluminum powder to improve explosive performance include Ammonal (67/22/11 wt% TNT/AN/Al), Minol-2 (40/40/20), and Tritonal (80/0/20) [55]. The aluminum is often assumed to only react with oxidizers in the detonation products (i.e., carbon dioxide, carbon monoxide, and water vapour) of explosives such as ANFO used in mining applications, or with oxygen in

atmospheric air [1, 77]. In a more modern context, aluminum nanopowders down to the ∼30 nm scale have become more commercially available, renewing the interest in the reaction of aluminum in explosives due to their high specific surface area and, consequently, enhanced reactivity. Kato and Murata [78] showed that aluminum particles with a mean diameter of 3 µm may react within microseconds and contribute to higher pressures close to the reaction zone, with results shown in Figure 2.5. Methods of measurement of the extent of aluminum reaction in the post-shock region include luminosity measurements using high speed imaging or photodiodes [76, 79], pressure measurements [78], and measurements of electrical conductivity [80–82]. The apparent delay in aluminum reaction behind the detonation front may be inferred from high-speed photography as shown in Figure 2.5, but the visual indicators may overestimate the actual ignition delay due to the opacity of the shattered glass fragments form the charge casing.

Work by Frost et al. [83–85] studied the reaction of packed beds of aluminum and magnesium particles saturated with sensitized NM to experimentally investigate the timescales of combustion and energy contribution of the aluminum reaction with the detonation products to the blast wave. Tanguay [86] developed a simplified 1D model to investigate the particle ignition reaction timescales of single particles in detonation reaction products. The model did not consider deformation of the particle, but determined that the surface reaction of the particle accounts for a small fraction of a percent of energy used to heat the particle, and found that most of the particle heating occurred during the Taylor

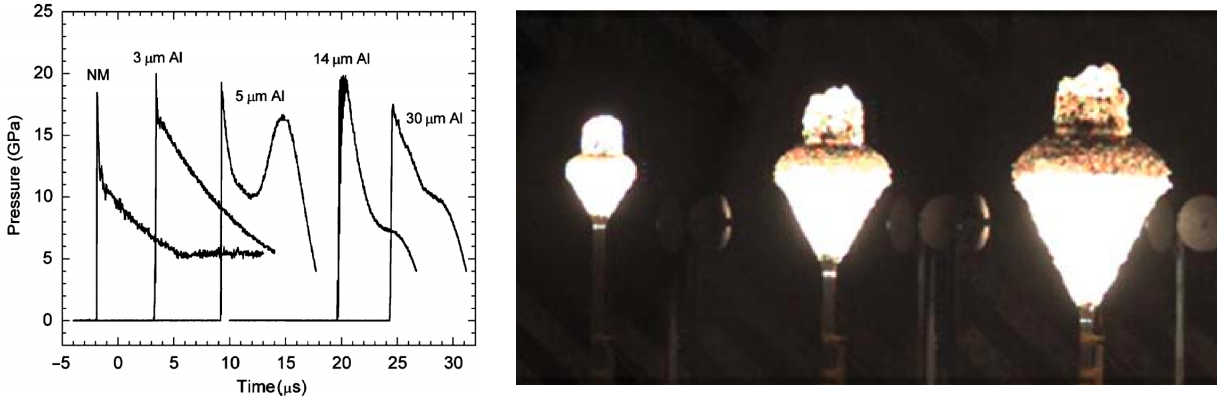

Figure 2.5: Left: Pressure-time profiles of detonation of NM and NM-Al mixtures of varying particle size, from Kato et al. [78]. Right: Still frames showing detonation and delayed luminosity of 3 µm aluminum particles in NM indicating a reaction onset time of 15 µs, from [76]. The data on the left does not correspond to the experiments on the right. Direct comparison of the results of both experiments cannot be made, in this case, as experimental parameters such as Al mass fraction and charge diameter are dissimilar.

expansion wave of the reacted flow. The model consequently overpredicted the critical charge diameter for prompt particle ignition for all particle sizes when compared to experimental results.

In the detonation environment, the thermophysical interaction of aluminum particles with the flow remains poorly understood, with a variety of physical phenomena playing a role, including: complete protection of the aluminum due to the oxide coating [87], particle deformation under shock loading potentially exposing aluminum in the nanosecond timescales of the shock front [56], slip between the flow and partially melted Al particles causing droplet breakup and shedding [88], and particle reaction delay depending on the

rate of particle heating [4]. Experiments which involve flyer-plate impact-delivered shock loading of aluminum particles, simulating the incident detonation shock in an inert medium, has demonstrated that significant particle deformation occurs for spherical Al particles and complete breakup of flake-Al particles [89], suggesting that deformation occurs due to the incident shock loading on the particle. Additionally, in the supercritical water regime, enhancement of the transport properties of water have been shown to dramatically increase the reaction efficiency of water with Al particles [59]. It is evident that no consensus has been reached on the complex mechanisms of the particle-flow interaction in the detonation regime.

2.5 Aluminum/Water Propellants

Modern interest in the aluminum-water system has been driven by the commercial availability of nanometric aluminum. The small particle size of the nano-Al promised to increase reactivity and reaction rate sufficiently to formulate worthwhile propellants. Propellants are of relevance to explosives as propellants, which similarly form gaseous products through highly exothermic deflagration, often support combustion in the detonation mode when initiated with a strong shock. Ivanov [90] discovered the potential to sustain deflagration in mixtures of nanoscale aluminum and water with a dilute 3 wt% polyacrylamide gellant. Risha et al. [91] conducted mass-burning rate tests of nano-Al in pure water. Sabourin [92] continued this work and noted the enhanced burning rate with

the addition of hydrogen peroxide fractions. Safety characterizations by Sippel et al. [13] in support of applied rocket propellant development demonstrated the potential to detonate nano-Al/ice mixtures using small-scale plate dent tests.

2.6 Aluminum/Water Detonation Reactions

Rozner and Holden [93] reviewed the literature on fast reactions of aluminum and water and noted prior studies by Shidlovskij [94], and Medard [95] that indicated the detonability of mixtures containing primarily aluminum and water. Medard tested suspensions of aluminum powder with particle size below 100 µm and water in 35 mm diameter cylinders [95]. Though the pure aluminum-water mixtures did not detonate, they became detonable when seeded with 7 wt% of the sensitive secondary PETN explosive. PETN-sensitized mixtures had detonation velocities of $3\,\mathrm{km\,s^{-1}}$. Medard conducted earthmoving tests with these mixtures and found that they made slightly smaller craters than equivalent TNT charges [95].

Recently, Schmitt et al. [15] observed self-sustained detonation in near-stoichiometric mixtures of nanometric aluminum particles with aqueous hydrogen peroxide (H_2O_2) in water. The charges were polyethylene-cased rate stick tests of various diameters to assess the detonability and critical diameter of the nano-Al/water-H_2O_2 system. Dilute, 10 wt% solutions of hydrogen peroxide were used in all tests. The mixtures were initiated using a HE booster and propagated at steady detonation velocities of approximately 3.0–3.2 $\mathrm{km\,s^{-1}}$ for tube diameters of 41.7 mm and 34.5 mm, low when compared to the detonation velocity

of conventional HEs. Detonation failed in 27.7 mm diameter tubes.

While high test hydrogen peroxide fractions (90 %+) have been known to be detonable alone or mixed with fuels [96,97], hydrogen peroxide in the current mixture is only present in a dilute quantity, indicating that the majority of the heat release supporting the detonation reaction is from oxidation reactions of aluminum.

It is during the formation of Al_2O_3 by chemical condensation of suboxides when most energy release occurs; this reaction is strongly exothermic whereas intermediate suboxide formation is weakly exothermic or endothermic. A list of the heat of formation of aluminum oxides and suboxides is presented in Table 2.2.

Oxide	ΔH_f^0, kJ mol^{-1}
$Al_2O_{3(s)}$	-1670
$AlO_{(g)}$	67.0
$AlO_{2(g)}$	-81.3
$Al_2O_{(g)}$	-144.1
$Al_2O_{2(g)}$	-405.7

Table 2.2: Specific heat of formation of aluminum oxides [98].

The mechanism by which hydrogen peroxide sensitizes the Al/water-H_2O_2 system to detonation is yet to be elucidated, but the production of oxygen-rich pores from hydrogen peroxide decomposition is likely involved. The oxygen pores present a multifaceted avenue for sensitisation; both physically and chemically. Similar to the addition of hollow glass microballoons (GMBs) or porous polystyrene balls in emulsion explosives, the catalytic decomposition of small fractions of aluminum powders and hydrogen peroxide has been

used in explosive formulations to sensitize explosive mixtures to detonation [99]. In addition to the fact that voids in the slurry act as hot spots, contents of voids chemically influence overall detonation parameters [100]. In Al/water-H_2O_2 strand burner tests, Sabourin et al. [92] found that the inclusion of hydrogen peroxide enhanced burning rates due to the catalysis on the aluminum oxide surface to yield molecular oxygen with faster oxidation kinetics than water vapour. Numerical combustion models by Storozhev et al. [101] indicate that the inclusion of even a small fraction of molecular oxygen (less than 3 mol %) can significantly accelerate the combustion of an aluminum-water vapour system by providing prompt pathways for the endothermic suboxide reaction $Al + O_2 \rightarrow AlO + O$. In high pressure heterogeneous shock tube experiments by Bazyn et al. [26], it was found that in atmospheres of molecular oxygen, water vapour, and carbon dioxide, disassociation of H_2O and CO_2 at high pressures to form more reactive oxides (O, OH, O_2) is potentially inhibited at higher pressure, leading to an increase in aluminum burn time for higher pressures for H_2O and CO_2, while atmospheres containing O_2 saw an increased burning rate, due to facilitated oxygen diffusion to the aluminum at higher pressures. However, it is important to note that the pressures tested in these experiments remain significantly lower than those in detonation conditions.

The possibility of detonating the Al/water-H_2O_2 mixture implies that the aluminum particles release their energy on a timescale on the order of less than 10 µs to support the detonation propagation, even if a fraction of the aluminum does not completely react

during this timescale. The mechanism responsible for this rapid release of energy under these extreme conditions is completely unknown at this point. The study of this binary explosive presents an avenue for probing the fundamental timescales of the aluminum-detonation product reaction and may potentially be used to accelerate the reactivity of aluminum in more conventional explosives.

Chapter 3

Experimental

This chapter discusses the materials and experimental methods used in the work presented in this thesis. The main experiment performed is the so-called rate stick experiment, in which a conventional HE booster, itself initiated with a detonator, is used to initiate detonation in a long cylindrical charge containing the insensitive test mixture through shock to detonation initiation [102]. Instrumentation is used to measure shock velocity along the length of the cylinder (VoD) and longitudinal wall velocity (cylinder expansion perpendicular to the direction of the detonation).

In general, rate stick investigations can be used to quantify the diameter effect and failure diameter of explosives. The diameter effect of an explosive refers to the dependence of the detonation velocity of the explosive on the charge diameter. The failure diameter of an explosive is the largest diameter at which detonation fails to propagate through the explosive,

and is dependent on the material used to confine the explosive charge. In this thesis, rate stick investigations were carried out to gauge detonability and detonation properties of Al/water-H_2O_2-filled charges. An number of tests was carried out to characterise the diameter effect or the failure diameter due to variations in charge density between tests due to the time-dependent expansion of the mixture.

The use of a HE booster to initiate an insensitive high explosive in rate stick experiments is a common cause of the initial overdriven detonation wave, produced when the detonation wave from the high explosive booster is transmitted into a lower detonation velocity explosive and a steady-state detonation reaction zone structure has not yet developed. As the transmitted shock decays, behind the shock accelerating chemical reactions occur, which eventually catch up to the shock, creating an overdriven detonation. After sufficient travel distance, the detonation wave will have decayed to a final steady state detonation velocity [102, 103]. As the run up distance of overdrive from the booster is uncertain in the novel explosive, x-t measurements of VoD are conducted as far as possible along the charge from the booster.

Shock pins were used to determine shock front time of arrival to measure VoD. Shock pins, also known as 'position transducers', are probes containing a small amount of pressure-sensitive material which produce an electrical signal when impacted at its sensing end by a fast moving object, or when exposed to a shock front [104]. Due to the low detonation velocity of the Al/water-H_2O_2 mixture, shock pins were placed internally for aluminum-

encased charges as the sound speed of the aluminum casing ($3.1\,\mathrm{km\,s^{-1}}$) is comparable to or may exceed the detonation velocity of the explosive test mixture ($\sim 3\,\mathrm{km\,s^{-1}}$). In this subsonic case, shock pins may prematurely detect acoustic waves travelling in the confining material if directly coupled to the aluminum casing. Shock pins were placed on the exterior surface of the charge cylinders confined with PVC casing (sound speed $\sim 1\,\mathrm{km\,s^{-1}}$).

Photonic Doppler velocimetry (PDV) is a technique used to measure the velocity of a moving surface. In PDV, laser light of a known wavelength is projected onto a surface. The reflected light is Doppler-shifted due to the surface movement and collected, where it is multiplexed with the source light to form a beat frequency capable of being measured using an oscilloscope. A discrete-time Fourier transformation of the beat signal reveals the surface velocity history. An excellent review of the history of PDV, description of the technique, and an in-depth presentation of the PDV instrumentation used in this thesis is presented by Loiseau [105].

3.1 Materials

As large-scale charge tests were performed in the present study, safety was an important consideration; less reactive coated powders were tested instead of the naturally oxidized aluminum used in previous studies. Two aluminum powders were mixed with oxidizing solutions: a nano-Al (V-ALEX) of $91 \pm 27\,\mathrm{nm}$ nominal particle diameter coated in the fluoroelastomer Viton, and a flake-Al (LED 1708AR) coated in trimethylolpropane

trimethacrylate (TRIM). The powders were obtained from Advanced Powder Technologies LLC., and Silberline Manufacturing Company Inc., respectively.

The V-ALEX powder contains the approximate composition by weight: Al: 85–87 % Oxides: 5–7 % Viton: 8–10 %. The V-ALEX particles are heavily agglomerated in bulk and form small branching agglomerates even when dispersed, as shown in Figure 3.1. The specific surface area of the nano-Al powder was estimated[1] to be 19–35 m^2/g.

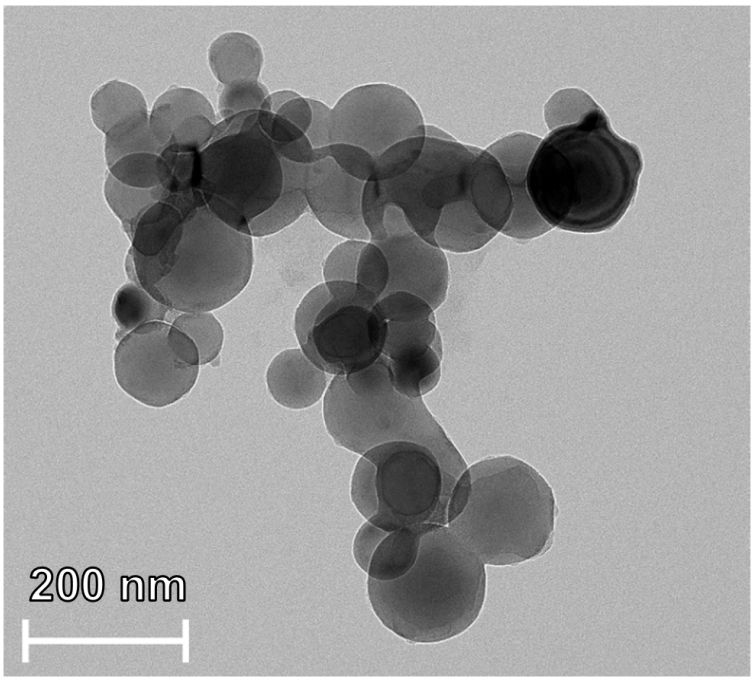

Figure 3.1: TEM image of small-scale agglomerate of V-ALEX, courtesy of Keena Trowell.

The flake-Al powder contains the approximate composition by weight: Al: 89.78 % TRIM: 10.24 % Teflon: 0.15 %. The flake is shown in Figure 3.2. The nominal diameter specified

[1]The formula for the specific surface area of a spherical volume of radius r and density ρ is SSA $= 3/\rho r$.

by the manufacturer is 20 µm. A Brunauer-Emmett-Teller test of specific surface area was performed with a Micromeritics Tristar 3000 using multipoint nitrogen adsorption ($p/p_0 =$ 0.0665–0.1994, $C = 18.1302$). The test determined a specific surface area of 5.09 m^2/g for the flake aluminum. Assuming the flake had the shape of a thin circular disk, the flake thickness was estimated to be 170 nm, with an aspect ratio of ∼120 typical for commercial flake powders.

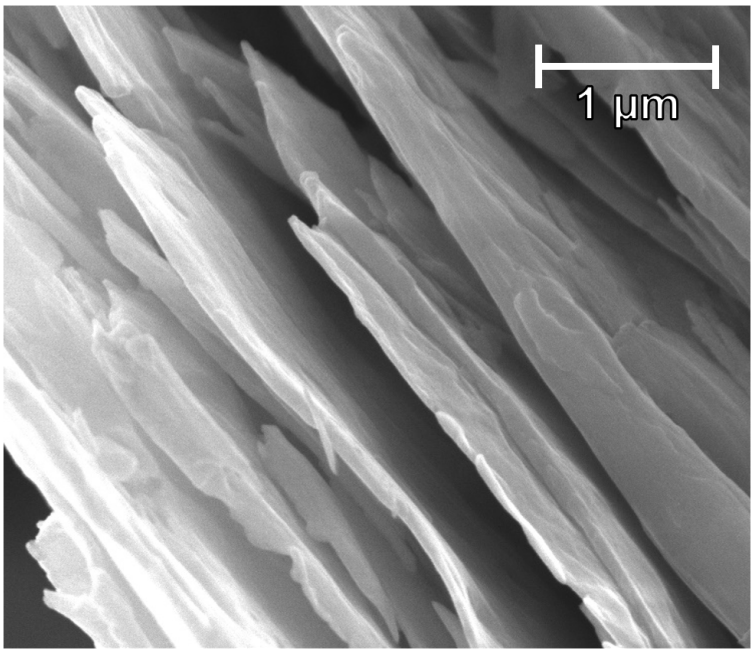

Figure 3.2: SEM image of flake-Al particles in profile view.

Two additional aluminum powders, an uncoated nano-Al (U-ALEX, Advanced Powder Technologies LLC.) and a micro-Al powder (H-1, Valimet Inc.) of 90–110 nm and 3.5 µm particle diameter, respectively, were considered for use. The U-ALEX powder was determined in preliminary safety testing to be too reactive in water for short-term storage,

and all trials with H-1 powders failed to sustain detonation.

Aqueous solutions of 5–20 wt% H_2O_2 were prepared from 30 wt% H_2O_2 (MilliporeSigma Canada Co.) diluted to lower concentrations using distilled water prior to mixing with aluminum powders.

For tests including flake-Al, a small amount of Rhodasurf 91-6 (Rhodia Canada Inc.), a surfactant, was added. The addition of this surfactant was necessary to obtain a homogeneous suspension of the aluminum flakes with the water-H_2O_2 solution and eliminated any visible agglomeration of the flake aluminum.

GMBs of 65 µm mean particle size (K1 Glass Bubbles, 3M Canada Co.) and prilled AN (MilliporeSigma Canada Co.) were used in sensitization investigations.

3.2 Aluminum/Water-H_2O_2 Mixtures

Initially, two nano-aluminum powders were considered: the fluoroelastomer-coated V-ALEX, and the uncoated U-ALEX. A safety assessment was performed by placing 0.5 g of nano-Al and 1.0 g aqueous hydrogen peroxide solution, mixed using a Hielscher UP50H ultrasonic processor, into a closed vessel at approximately 35 °C and recording the pressure rise associated with the formation of gaseous oxygen and hydrogen products. The 2:1 ratio of aqueous solution to powder was used to provide excess water to ensure a high reaction efficiency for the aluminum-water reaction. Figure 3.3 shows the gas evolution for the two nano-Al powders mixed with aqueous solutions of 10–15 wt% H_2O_2. Solution strength is

reported as the weight fraction of hydrogen peroxide in water.

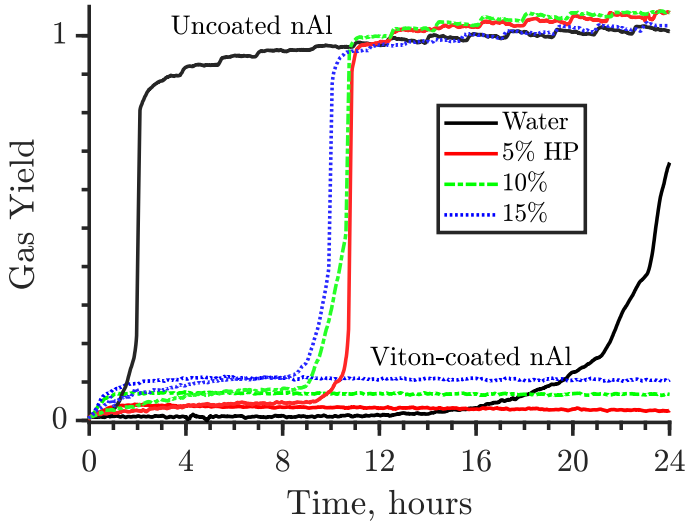

Figure 3.3: Gas evolution for mixtures of U-ALEX and V-ALEX and water or diluted hydrogen peroxide solutions. Gas yield is normalized by the expected yield of the $2\,Al + 3\,H_2O \rightarrow Al_2O_3 + 3\,H_2$ reaction.

In pure water, reaction of the uncoated U-ALEX was prompt, leading to the explosive production of hydrogen within 1 hour of mixing. The addition of only 5 wt% H_2O_2 to the solution suppressed substantial aluminum oxidation for nearly 10 hours, after which the mixture reacted explosively. Additions of hydrogen peroxide retained this suppressive effect, but incrementally increased early gas yield.

The surface coating on the V-ALEX delayed the onset of the aluminum-water reaction. When mixed with pure water, no gas was produced for around 12 hours, after which accelerating reaction was observed. The addition of hydrogen peroxide suppressed rapid

reaction for the entire duration of measurement (nearly 24 hours). So, while the Viton coating reduced reactivity, it did not provide complete protection for the particles. Exothermic heating at localized failures in the coating likely compromised neighbouring coating, leading to extensive reaction. Increasing fractions of hydrogen peroxide beyond 5 wt% again yielded incremental increases in gas production for the V-ALEX.

We postulate that two competing effects are responsible for the moderating effect of hydrogen peroxide. The addition of hydrogen peroxide to water suppresses the formation of OH^- and thereby indirectly limits the reaction of the nano-Al with water [106]. While the presence of hydrogen peroxide moderates the main reaction of nano-Al with water, it is decomposed by the ceramic oxide coating on the particle surface yielding predominantly oxygen gas [107]. Consequently, higher concentrations of hydrogen peroxide evolved greater gas yields.

Reactivity tests repeated with flake-Al did not react explosively to form hydrogen gas in any cases, including the pure water solution. The aluminum-water reaction is likely quenched due to heat loss resulting from the larger size of the aluminum flake in addition to the TRIM coating. As observed in nano-Al tests, incremental increases in hydrogen peroxide content yielded proportional increases in gas production, indicating that the flake-Al also had exposed oxide surface area.

The spontaneity and violence of the nano-Al/water reactions introduced hazards in charge preparation. Unlike prior studies, relatively large masses of mixture (>500 g) were

to be placed in metal confinement, increasing the hazard in the event of reaction. U-ALEX mixtures were deemed unsafe for use in these experiments as large quantities of hydrogen could be generated within an hour of preparation. Only the V-ALEX nanopowder was used for further tests as the passivating Viton coating was deemed to sufficiently delay substantial reaction. To further mitigate risk, mixture batches were prepared using chilled water and then promptly poured into the charge cylinders. Tests prepared ex situ were stored in a freezer at $-18\,^{\circ}\mathrm{C}$ until use and allowed to thaw prior to firing.

The measure of gaseous product evolved taken prior to the onset of significant hydrogen production versus initial amount of hydrogen peroxide is plotted in Figure 3.4 for the V-ALEX, U-ALEX, and flake-Al reactivity tests. In all cases, the product gases follow $H_2O_2 \rightarrow \frac{1}{2}O_2$, demonstrating complete thermal decomposition of the hydrogen peroxide to oxygen and water, as observed in a previous study investigating the decomposition of hydrogen peroxide on pure ceramic oxides [107]. Deviations higher from this trend may be attributed to early production of hydrogen gas of the uncoated U-ALEX.

Approximately stoichiometric mixtures of Al/water-H_2O_2 expanded significantly over time due to gas production in the slurry entrained as porosity. To elucidate the content and time-dependence of void formation in trials with flake aluminum, expansion tests were performed for mixtures of flake-Al/water-H_2O_2 of varying hydrogen peroxide concentration using preparation methods identical to those used to formulate the explosive mixtures investigated in this study. The mixtures were placed in a graduated cylinder and the time

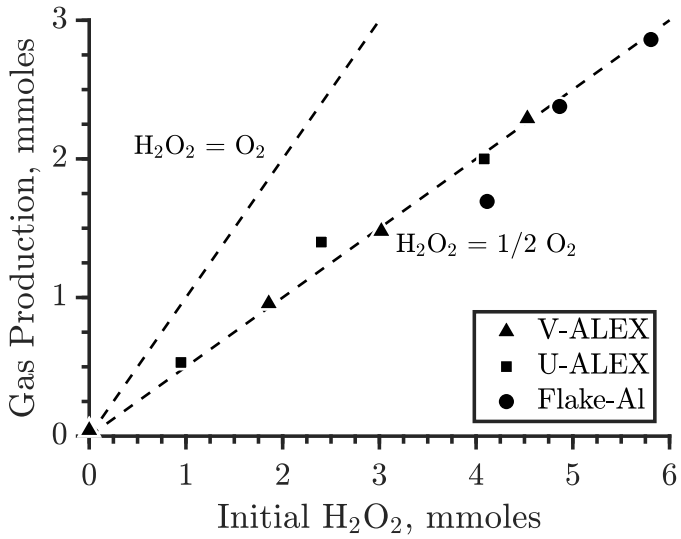

Figure 3.4: Production of gaseous O_2 products as a function of initial H_2O_2 concentration prior to explosive hydrogen production. The dashed lines show the expected amount of O_2 for different stoichiometries.

evolution of slurry volume and mass was monitored. The results of expansion tests are shown in Figure 3.5. These tests were used to provide estimates of the unfrozen slurry expansion progress and demonstrate that increased peroxide fractions result in decreased density in explosive mixtures.

In all cases the mixtures had an initial density of ∼90 % theoretical maximum density (TMD). This initial porosity is likely stemming from entrapped air, gaseous oxygen or hydrogen formation during mixing, or particle agglomeration, although no agglomerations on the scale of those observed in the bulk powder were visible after acoustic mixing. Mixtures containing pure water did not develop further porosity during the measured time,

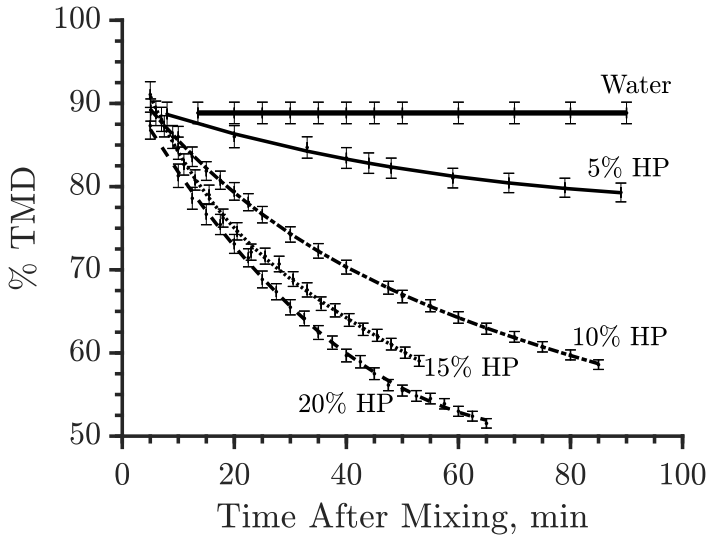

Figure 3.5: Density evolution of mixtures of flake-Al powder and solutions of 0, 5, 10, 15 and 20 wt% H_2O_2 in water, with TMD of 1.401/1.415/1.432/ 1.450/1.468 g cm^{-3}, respectively.

while mixtures containing 5–20 wt% H_2O_2 demonstrated incremental decreases in density. The results indicate that further mixture expansion is due to the product oxygen from the decomposition of the hydrogen peroxide. Only a small fraction ($\sim$2 %) of the hydrogen peroxide developed into entrained porosity, as observed in [15].

3.3 Mixture Preparation

For charge preparation, similar to prior works [13,15,91,92], acoustic mixing was required to achieve acceptable dispersion of the nano-Al in the aqueous solutions. A Resodyne LabRAM resonant acoustic mixer was used to prepare all mixture batches. The limited capacity of the

LabRAM mixing jars dictated that each charge had to be filled with two 165 g batches. Each batch was prepared by adding 75 g of V-ALEX and then 90 g of aqueous solution. The slurry was mixed by operating the LabRAM at 50 % intensity for 30 minutes, with the resultant mixture shown in Figure 3.6. Complications in mixing arose because the Viton coating was hydrophobic. Consequently, mixtures were prepared slightly fuel lean ($\phi \approx 0.8$). Visible particle agglomerates also remained on the jar walls after mixing.

Figure 3.6: Prepared V-ALEX/water-H_2O_2 mixture.

Similar to the nano-Al tests, a Resodyne LabRAM resonant acoustic mixer was used to prepare all mixtures of flake-Al in the aqueous solutions. Each charge was filled with multiple 200 g batches. Each batch was prepared by adding 100 g of flake-Al and then 100 g of aqueous solution ($\phi \approx 1.0$). Due to the hydrophobic TRIM coating, an additional 1.0 g of

surfactant Rhodasurf 91-6 was added to mixture batches to achieve a homogeneous slurry. The slurry was mixed by operating the LabRAM at 50 % intensity for 5 minutes, with the unmixed and resultant mixture shown in Figure 3.7.

Figure 3.7: Flake-Al mixture before (left) and after (right) acoustic mixing.

Charge cylinders were manually agitated after the addition of each mixture batch to release entrapped pockets of air. For shots #1–13, the prepared slurry was frozen after mixing, and fired after being defrosted. For shots #14–22, shots were fired within an hour of preparation. With inclusions of fractions of hydrogen peroxide, peroxide decomposition systematically reduced charge density with increasing peroxide fraction. When unfrozen, the slurry volume continued to vary. The mass of slurry inside the cylinder was measured prior to fitting the charge with the booster, an estimated 20 minutes before firing.

Additional trials varied fractions of hydrogen peroxide, AN and GMBs. Prilled AN was dissolved into water (e.g., 900 g water + 100 g AN) to form an aqueous solution prior to

mixing with flake-Al powder. GMBs were added during mixing of the flake-Al powder and aqueous solution.

3.4 Charge Design

Shots #1–7 were conducted using thick-walled (9.55 mm wall thickness) aluminum cylinders: 38.1 mm ID, 57.2 mm OD, and 203 mm long. Heavy metal confinement was chosen to help support the propagation of a detonation. The cylinder L/D was 5.3, substantially lower than the L/D $>$ 10 typical of precision rate sticks, as the cylinder length was constrained by nano-Al availability and the batch volume of the mixing equipment. However, cylinder length was sufficient to scope out detonability and roughly measure detonation velocity and accelerating ability. Shots #1–7 were initiated by a 100 g C-4 booster whose OD matched the ID of the charge cylinder.

A schematic of the charge used for shots #1–7 is given in Figure 3.8, and shown in Figure 3.9 instrumented with PDV collimators and fitted with a C-4 booster. The cylinders were sandwiched between two polyethylene plates. The purpose of the top plate was to mate the booster to the cylinder and to prevent booster fragments and products from interfering with the optical diagnostics. The bottom plate held brackets which housed optical collimators (Ningbo Snow Sea Electronic Commerce Co. Ltd.) in slots placed 50.8 mm apart for wall velocity measurements using PDV, with the first probe located 88.9 mm from the C-4 booster. The onset of wall motion recorded by the pair of PDV probes was used to calculate detonation

velocity.

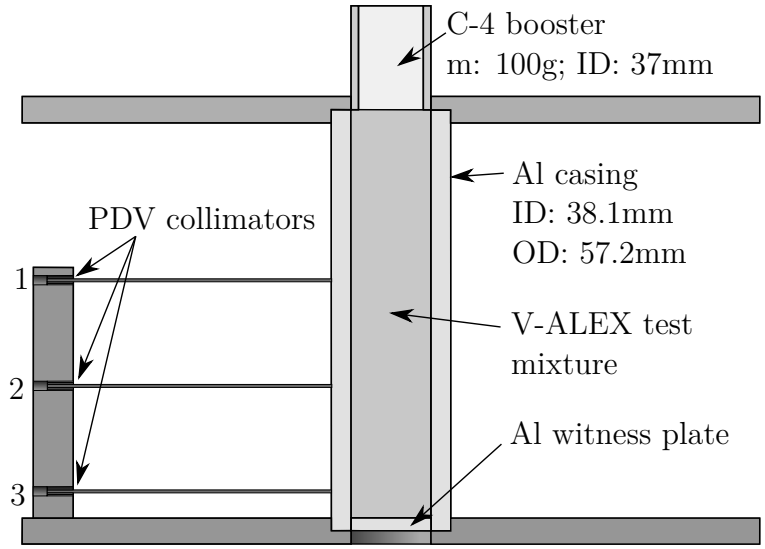

Figure 3.8: Charge geometry of shots #1–7.

As there is typically 1–3° of misalignment of the collimator lens, the laser spot locations were accurately measured (±0.2 mm) after the collimators were installed in the bracket. The collimators were spaced approximately 125 mm from the cylinder wall. There were three collimator stations along the mounting bracket. Only two stations were instrumented per experiment, yielding two wall velocity measurements at separate locations for each experiment. The stations were interchanged between repeat tests.

Shots #8–13 were encased in a larger diameter aluminum cylinder: 69.9 mm ID, 76.2 mm OD, and 356 mm long (L/D = 5.1) to support detonation. Shots #14–22 were confined in a PVC casing: 49.3 mm ID, 60.3 mm OD, 381 mm length (L/D = 7.7). Shots #8–22 were initiated using a pentolite booster (D = 50 mm, 454g). The charges of shots #8–13 and #14–

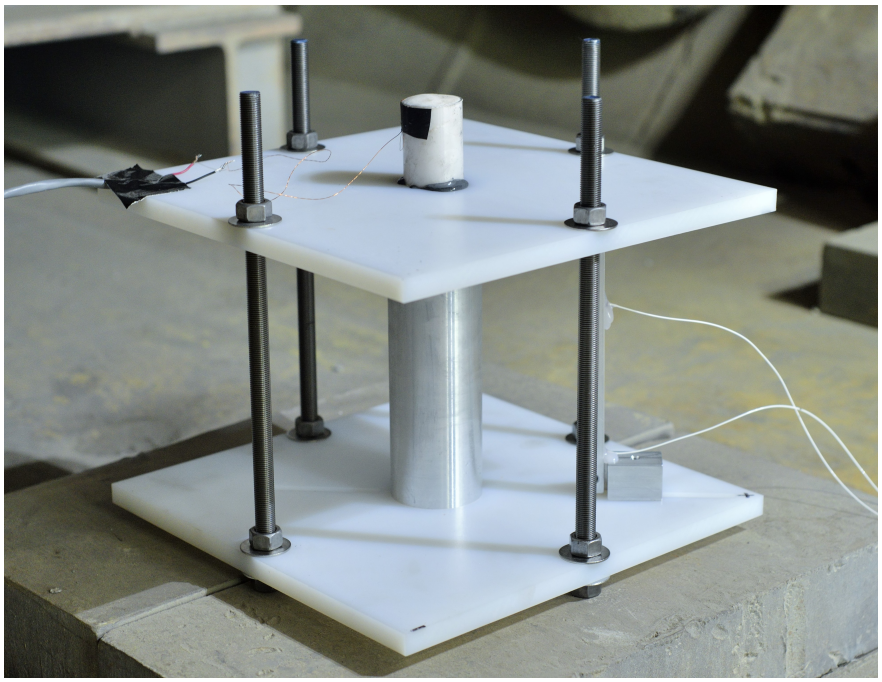

Figure 3.9: Assembled charge used in shots #1–7.

22 are illustrated in Figure 3.10 and shown in Figure 3.11, instrumented with shock pins and fitted with pentolite boosters. Four Shock Dynasen CA-1145 (Dynasen Inc.) piezoelectric shock pins were positioned 50.8 mm apart and inserted into the center of the cylinder (#8–13) or on the outside of the cylinder (#14–22). The first shock pin was located 140 mm and 203 mm from the booster in trials #8–13 and #14–22, respectively.

The HE boosters were pressed into the charges until resistance by the Al/water-H_2O_2 mixtures was felt. Twisted wire pairs pressed into the top of the booster were used to trigger diagnostics. For each test, an aluminum flyer witness plate was affixed to the base of each cylinder. Total fragmentation of the cylinder as well as deformation and pitting of the

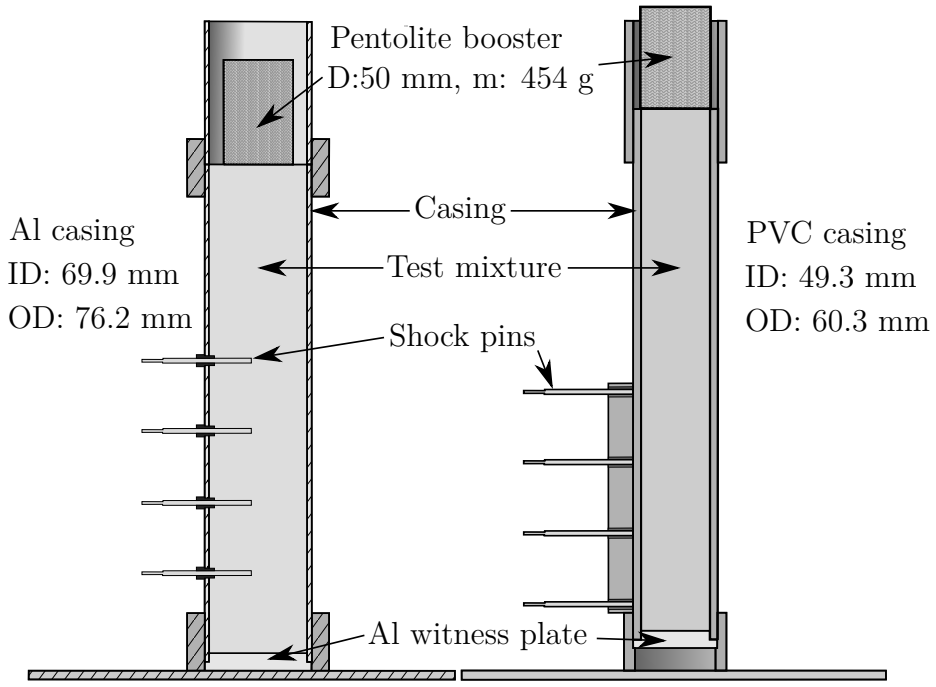

Figure 3.10: Charge geometry of shots #8–13 (left) and #14–22 (right).

witness plate was considered evidence of detonation.

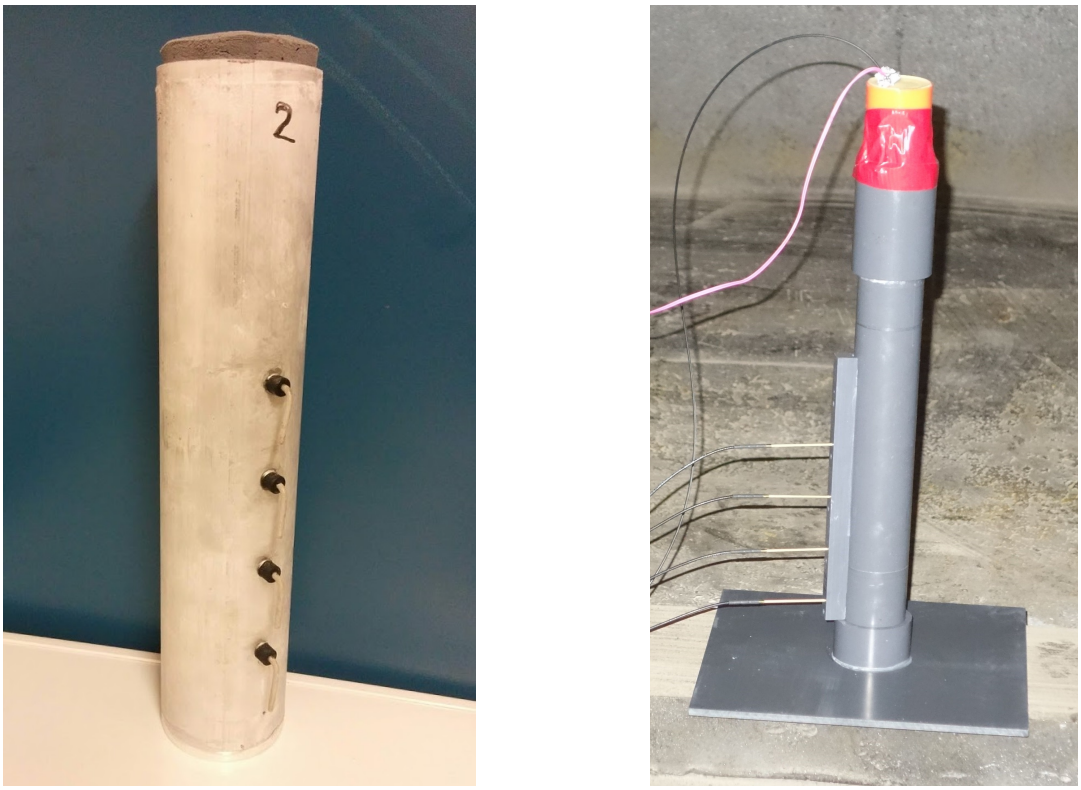

Figure 3.11: Charges used in shots #8–13 (left) and #14–22 (right).

Chapter 4

Results

4.1 Nano-Al/Water-H_2O_2 Mixtures

4.1.1 Detonation of Nano-Al/Water-H_2O_2

In total, 8 detonability tests were conducted for the nano-aluminum slurries. In smaller geometry cylinders, tests of V-ALEX and 0, 5, and 10 wt% H_2O_2 mixtures were conducted, each repeated once. A single test was conducted at 15 wt% H_2O_2. In a larger cylinder, one test was conducted with the 10 wt% H_2O_2 solution. Mixture properties and detonation velocities are reported in Table 4.1.

In smaller geometry tests, mixtures with 10 or 15 wt% H_2O_2 detonated along the entire length of the charge, and fully fragmented the cylinder. Mixtures with 0 or 5 wt% H_2O_2 clearly failed to detonate more than half-way down the length of the charge and the lower

Shot, #	Fuel	Oxidizer, wt% in H_2O	Confine-ment	ID, mm	ρ, $g\,cm^{-3}$	D, $km\,s^{-1}$
1	V-ALEX	-	Al	38.1	1.06	no-go
2	V-ALEX	-	Al	38.1	1.05	no-go
3	V-ALEX	5 % H_2O_2	Al	38.1	0.98	no-go
4	V-ALEX	5 % H_2O_2	Al	38.1	1.02	no-go
5	V-ALEX	10 % H_2O_2	Al	38.1	0.95	3.08
6	V-ALEX	10 % H_2O_2	Al	38.1	0.99	3.23
7	V-ALEX	15 % H_2O_2	Al	38.1	0.96	3.15
8	V-ALEX	10 % H_2O_2	Al	69.9	0.84	no-go
9	H-1	5 % H_2O_2	Al	69.9	1.48	no-go
10	H-1	10 % H_2O_2	Al	69.9	1.49	no-go
11	Flake	-	Al	69.9	1.33	no-go
12	Flake	5 % H_2O_2	Al	69.9	1.27	no-go
13	Flake	10 % H_2O_2	Al	69.9	1.06	3.45
14	Flake	7.5 % H_2O_2	PVC	49.3	1.26	no-go
15	Flake	7.5 % H_2O_2 + 1 % GMB	PVC	49.3	1.22	no-go
16	Flake	10 % H_2O_2	PVC	49.3	0.98	2.98
17	Flake	10 % H_2O_2	PVC	49.3	1.15	no-go
18	Flake	15 % H_2O_2	PVC	49.3	1.03	2.94
19	Flake	20 % H_2O_2	PVC	49.3	0.93	2.76
20	Flake	10 % AN	PVC	49.3	1.38	no-go
21	Flake	20 % AN + 1 % GMB	PVC	49.3	1.34	no-go
22	Flake	1 % GMB	PVC	49.3	1.26	no-go

Table 4.1: Summary of detonation experiments. Weights are tabulated by percent mass in the aqueous solution. Densities are reported as measured.

third of the cylinders were recovered intact. Figure 4.1 shows the recovered case fragments from these nano-Al-containing charges. With increasing hydrogen peroxide content, smaller case fragments were recovered. The larger fragments contained unreacted nano-Al mixture. No substantial difference in case fragment sizes were recorded between 10 and 15 wt% trials.

Figure 4.2 shows the pairs of PDV traces for experiments where the detonation was

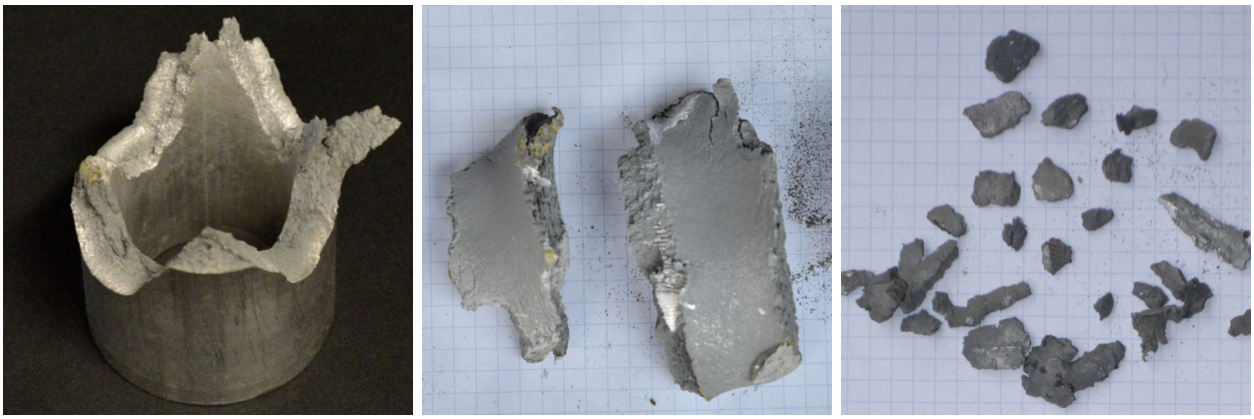

(a) Water **(b)** 5 % H_2O_2 **(c)** 10 % H_2O_2

Figure 4.1: Recovered case fragments from trials containing mixtures of nano-Al.

deemed to have failed (0 and 5 wt% H_2O_2). Figure 4.3 shows the pairs of PDV traces for the experiments deemed to have detonated the full length of the charge (10 and 15 wt% H_2O_2). Note that the times reported in these figures reflect the longitudinal positions of the collimators changing between stations in repeat shots, where the collimators were moved attempting to observe variation in the wall velocity profile.

The PDV signals were noisy and oscillatory compared to typical metal acceleration experiments. We attribute this to the short length and thick walls of the cylinder, resulting in complex wave interactions from the booster and charge ends. Nevertheless, the signals were reasonably reproducible for the three experiments that detonated. No sharp shock-breakouts at the free surface of the cylinder were observed, consistent with the subsonic detonation velocities. For detonating cases, wall velocity histories were similar at both ends of the cylinder. These results imply detonation until the end of the charge.

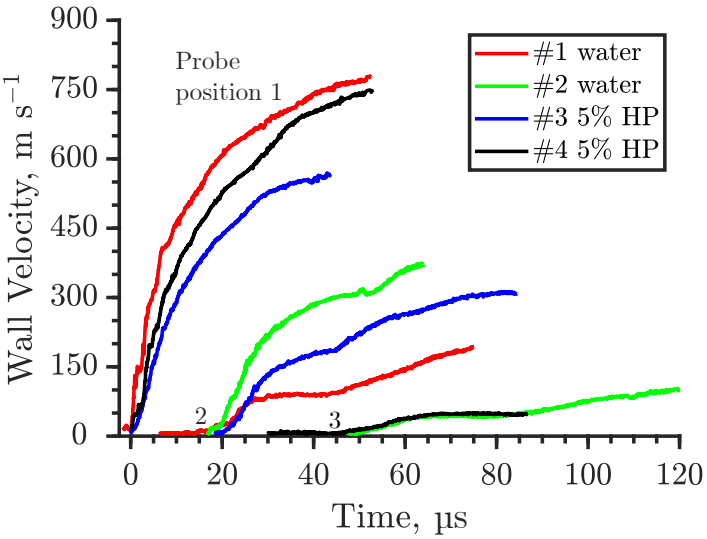

Figure 4.2: PDV velocity histories for 0 and 5 wt% H_2O_2 V-ALEX experiments that failed before the end of the charge.

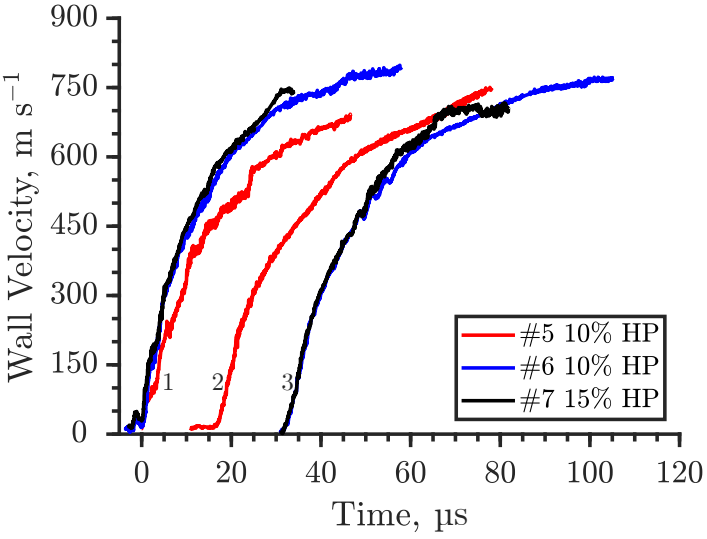

Figure 4.3: PDV velocity histories for 10 and 15 wt% H_2O_2 V-ALEX experiments that detonated until the end of the charge.

In all tests, the aluminum cylinder walls ruptured prematurely, and signals were lost before terminal velocity was reached. Maximum wall velocities for detonating charges #5–7 were found to be 749, 793, and 744 $\mathrm{m\,s^{-1}}$, respectively.

For non-detonating cases, the wall velocities obtained at the first probe position closest to the C-4 booster were similar to the velocities at the first probe position in detonating cases. However, wall velocities were substantially lower at the middle of the charge (as shown at 30 µs onwards in Figure 4.2). Wall velocities near the charge ends were even lower as the probes were aimed at a location just above where the fragments tore off from the intact length of the cylinder. The reduction in wall velocity provides evidence of detonation failure.

Propagation velocities were calculated to be 3.1–3.2 $\mathrm{km\,s^{-1}}$. With only two x-t points, the degree of overdrive from the C-4 booster cannot be ascertained, however the reported detonation velocities are close to prior literature values [15].

4.2 Flake-Al Mixtures

4.2.1 Detonation of Flake-Al/Water-H_2O_2

The detonability of flake-Al/water-solution mixtures in cylindrical charges was investigated. In total, 8 tests were conducted for different flake-Al/water-H_2O_2 compositions. In 49.3 mm diameter cylinders, tests were conducted with flake-Al mixed with 7.5, 10, 15 and 20 wt%

H_2O_2, with the 10 wt% H_2O_2 case repeated once. In 69.9 mm diameter cylinders, tests were conducted with 0, 5, and 10 wt% H_2O_2 solution. The parameters for each test are given in Table 4.1. Mixtures with 15 or 20 wt% H_2O_2 detonated along the entire length of the charge. Two mixtures of 10 wt% H_2O_2 succeeded and one mixture failed in sustaining detonation. Mixtures with 0, 5, or 7.5 wt% H_2O_2 clearly failed to detonate part-way down the length of the charge and the lower half of the cylinders were recovered intact.

For the detonating cases, the shock pins registered a consistent high shock velocity down the cylinder. For the non-detonating cases, a shock wave was observed with decaying velocity much lower than the detonation velocity of detonating cases. Propagation velocities of detonating shots were calculated to be 2.8–3.5 $\mathrm{km\,s^{-1}}$ and are shown in Figure 4.4. No overdrive from the charge booster is observed as shock pins were located far from the booster, evidenced by a constant or increasing shock velocity. Despite the morphological difference in larger flake- and nano-aluminum powders, the reported velocities are congruent with values reported in the nano-aluminum formulations [15].

4.2.2 Detonation of Other Flake-Al Mixtures

Attempts to elucidate the mechanism of detonation were carried out with 4 further tests conducted for different compositions in 49.3 mm diameter cylinders. Tests (#18, #20–22, Table 1) were conducted with the inclusion of GMBs and AN. To determine if dilute additions of an energetic strong oxidizer may act as a sensitizer to aluminum-water mixtures, as may

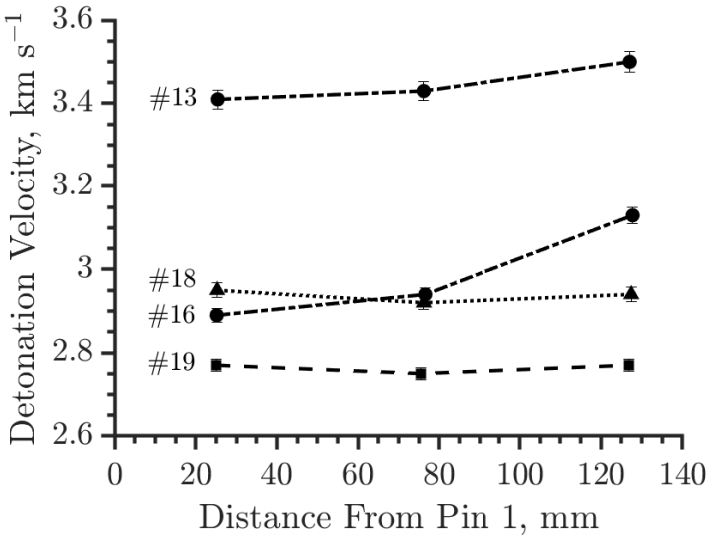

Figure 4.4: Shock velocity variation along length of detonated flake-Al shots.

be occurring with the hydrogen peroxide, 10–20 wt% AN was added to the aqueous solution. A small fraction of 1 wt% GMBs was added to formulations to increase porosity, however, the addition of GMBs during charge preparation did not reduce the density to that observed in detonable tests containing hydrogen peroxide. All such mixtures failed to sustain detonation.

4.3 Micro-Al/Water-H_2O_2 Mixtures

Two tests (#9 and #10, Table 4.1) were attempted using the 3.5 µm uncoated H-1 micro-Al powder. To avoid settling of the larger aluminum particles, 2 wt% of a poly-(acrylamide-co-acrylic acid) thickening agent (MW = 5,000,000, CAS Number 9003-06-9, Aldrich Chemical Company Inc.) was used. The thickened water was mixed with peroxide to form the final

gelled aqueous solution, mixed with equal weight of H-1 powder, and frozen to avoid settling and thermal cook-off before testing. Shots prepared with H-1 failed to sustain detonation.

Chapter 5

Discussion

It is likely that a large fraction of the aluminum is not reacting sufficiently quickly before the sonic plane to contribute to the detonation propagation. The equilibrium code Cheetah 2.0 with the BKWC product library was used to estimate the detonation velocity for mixture compositions containing 10–20 wt% H_2O_2 solution with a varying percentage of the aluminum reacting in the detonation sonic plane. Selected details of the Cheetah-estimated properties are provided in Appendix A, and inputs for the calculations are provided in Appendix B. Cheetah-calculated detonation velocities are plotted alongside experimental results in Figure 5.1 against a varying density resulting from evolution of gaseous oxygen. The smooth curves are detonation velocities determined using Cheetah for varying fractions of reacting aluminum. Fractions of reacting aluminum less than 40 % failed to converge to a solution in Cheetah. Calculations indicate a small effect of the small

variation of hydrogen peroxide concentration on the detonation velocity. Data points are experimental results from the current Al/water-H_2O_2 tests.

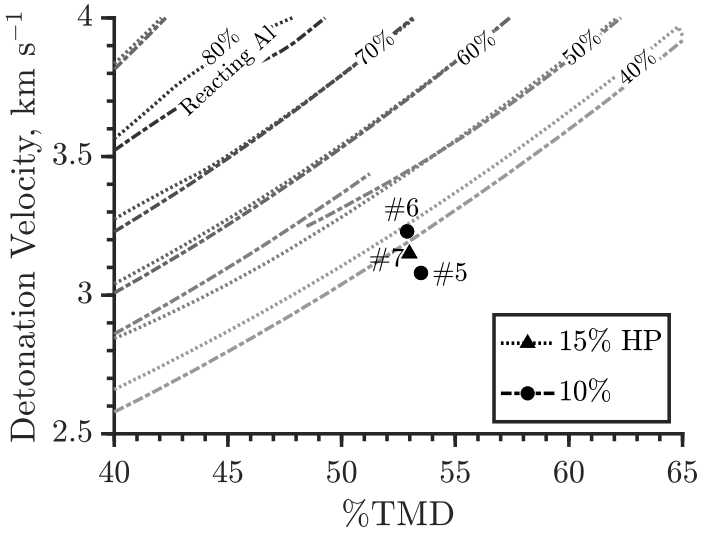

Figure 5.1: Comparison of experimental results of nano-Al/water-H_2O_2 detonation and results calculated by Cheetah 2.0.

From simple integration of the PDV signals, a maximum of 6.1 relative volumes of expansion was reached prior to rupture. Although wall velocities were not fully terminal, the Gurney velocity of the mixture was estimated based on the maximum terminal velocities obtained. Gurney's equation for a cylinder was used [55]:

$$V_{\text{wall}} = \sqrt{2E}\left(\frac{M}{C} + \frac{1}{2}\right)^{-1/2}$$

V_{wall} is the maximum recorded wall velocity, M was taken to be the average mixture mass for the 10 and 15 wt% H_2O_2 experiments, C is the mass of the cylinders, and $\sqrt{2E}$ is the

Gurney velocity coefficient. The Gurney velocity coefficient was estimated to be $1.62\,\mathrm{km\,s^{-1}}$. This value is considerably lower that what is obtained for typical military explosives, however the geometry used for the present tests was non-standard, resulting in early wall rupture and termination of the PDV measurement.

Using the analytical approach derived by Jackson, [108] (with the corrected kinematics for the cylinder analysis of [109]), the product expansion P-ν behaviour was estimated based on the wall motion of charge #6, which provided the longest duration and smoothest non-interrupted signal. In this analysis, incompressible case motion was assumed due to the relatively low detonation pressures of the non-ideal explosive. A low-pass filtering technique was used to reduce signal noise while preserving early time information, however due to the oscillatory PDV signals, large oscillations were observed in the resultant P-ν behaviour. To smooth the data further, the data were fit by the analytic form described by Davis and Hill [110] known as the 'Hill Fit'. The resultant product P-ν behaviour is plotted in Figure 5.2, alongside the computed product JWL isentropes from Cheetah 2.0 assuming 30–50 and 100 % fractions of reacting aluminum, using the BKWC product library. As observed in a similar analysis for ANFO cylinder expansion tests [109], a discrepancy exists between the measured and predicted isentrope assuming 100% combustion. This is attributed to incomplete combustion of the aluminized explosive. As the Hill-fit P-ν evolution of the expanding products follows the 40 % Cheetah-derived isentrope, little to no post-detonation reaction is discerned.

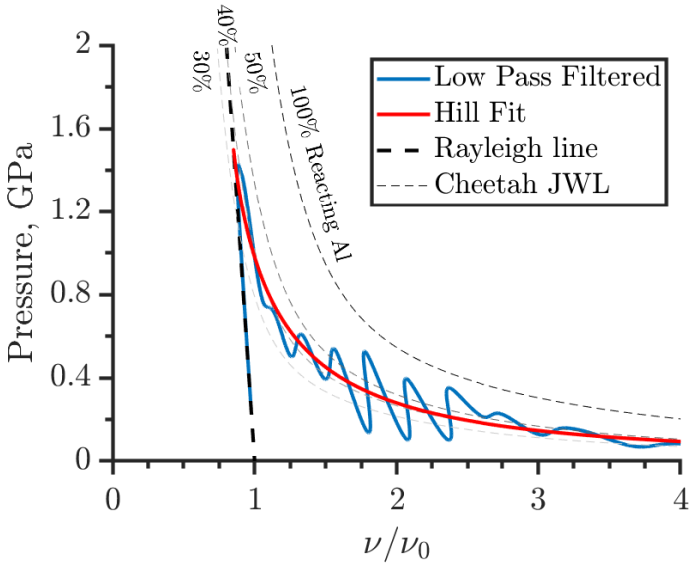

Figure 5.2: Experimentally measured P-ν evolution of the nano-Al system products compared to the predicted JWL-fit product isentropes by Cheetah.

The results for the flake-Al system tests are plotted with Cheetah-reported velocities in Figure 5.3. As charges exhibited expansion after density measurement, X-error bars are estimated density evolution from the measured point (errorbar at rightmost extent) to predicted density (symbol at leftmost extent) based on expansion tests for time elapsed (approximately 20 minutes) between charge preparation and firing. Shot #13, prepared frozen, did not expand further prior to firing. Y-error bars are the extrema of inter-pin VoD variation. The experimental results are congruent with the calculated trend of increasing detonation velocity with density.

The experimental data follows the Cheetah-calculated detonation velocities where 40 % of the aluminum was assigned as reacting, for both flake- and nano-Al tests. A velocity

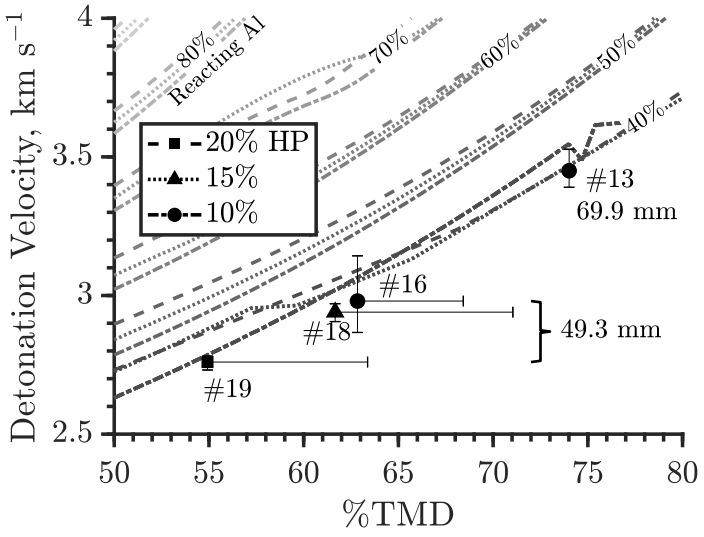

Figure 5.3: Comparison of experimental results of flake-Al/water-H_2O_2 detonation and results calculated by Cheetah 2.0.

deficit on the order of $2\,\mathrm{km\,s^{-1}}$ is observed when compared to the complete reaction, even in the largest diameters tested. We stress that the Cheetah-calculated results are potentially not indicative of the true nature of the velocity deficit and fraction of reacted aluminum due to the non-ideality of the heavily aluminized, binary explosive. Possible sources include incomplete reactant mixing, incomplete reaction at the sonic plane, diameter effects, or gaps in the knowledge of aluminum oxide chemistry. Due to loosely attached valence electrons, metals are extremely reactive with practically all known oxidizers. The activation energies of metal-oxidiser reactions are small, if positive at all, and for the aluminum-oxygen reactions are estimated to be below $500\,\mathrm{kcal\,mol^{-1}}$ [111]. Consequently, the reaction of aluminum with oxygen at elevated temperatures is limited practically not by reaction kinetics, but likely by

the physical processes of reactant mixing. A similar analysis using the BKWS product library estimated a 20–30 % reacting aluminum fraction.

The results indicate that the addition of weak hydrogen peroxide fractions sensitize the aluminium-water mixtures to detonation. Possible avenues of explosive sensitization include chemical sensitization, i.e., addition of hydrogen peroxide as an oxygen-rich energetic additive, or physical sensitization, brought on by the evolution of oxygen porosity from hydrogen peroxide's catalysed decomposition. Voids in the slurry may sensitize the mixture to detonation mechanically by the generation of hot spots following void collapse: fractions of aluminum powders and hydrogen peroxide have been used in patented explosive formulations [99], catalytically decomposing the hydrogen peroxide to form oxygen bubbles to sensitize the explosive mixtures to detonation. Additionally, the contents of the voids can influence detonation parameters chemically [100]. Sabourin [92] postulated that the inclusion of hydrogen peroxide enhanced aluminum-water strand burning rates due to resultant molecular oxygen with faster oxidation kinetics than water vapour. Combustion models by Storozhev [101] indicate that the inclusion of a small fraction of molecular oxygen can accelerate the combustion of the aluminum-water system by providing prompt pathways for weakly endothermic suboxide reactions.

However, in this work, insufficient and excess porosity each potentially resulted in chemically identical repeated trials to result in a 'no-go' where the formulation had previously been successful. Shot #17, which failed to sustain detonation, was a repetition

of shot #16, which did detonate. In shot #17, there was a shorter delay between shot preparation and firing, resulting in less decomposition of the hydrogen peroxide, and a higher overall density of the mixture. Shot #8, which failed to sustain a detonation through the length of the charge cylinder, was a repetition with larger charge geometry of shots #5 and #6, which detonated. Discrepancies in preparation occurred between the smaller and larger charges when freezing the mixture. When cooling, the larger charge, with larger thermal mass, developed increased porosity compared to the smaller charges. The resultant significantly lower density of the large-diameter test is likely ultimately responsible for the failure to sustain detonation. The difference in results of repeated trials indicate that it is not purely a thermochemical reliance on a higher hydrogen peroxide fraction to sensitize the mixture to detonation, but a physical void-sensitization effect. This non-reliance on the strong oxidizing fractions of hydrogen peroxide is further confirmed by the failure of mixtures containing fractions of another strong oxidizer, AN, to sustain detonation. These results indicate the possibility of detonating mixtures containing low ($<10\,\mathrm{wt}\%$) amounts of hydrogen peroxide, glass balloons, or polystyrene beads, if a critical mixture density is achieved.

Chapter 6

Conclusions

Self-sustained detonation was observed in 3 nano-Al/water-H_2O_2 mixtures and 4 flake-Al/water-H_2O_2 mixtures of density between approximately 0.81–1.06 $\mathrm{g\,cm^{-3}}$ where the fraction of hydrogen peroxide in the oxidizing solution was 10–20 wt%. Detonation velocities of 2.8–3.5 $\mathrm{km\,s^{-1}}$ were recorded. The Gurney velocity of the nano-Al/water-H_2O_2 system was estimated to be 1.64 $\mathrm{km\,s^{-1}}$ when cylinder walls ruptured at 6 relative volumes of expansion. We did not observe an effect of confinement on the detonability of mixtures tested in this study. No discernible effect of hydrogen peroxide content was observed either in propagation velocity or wall acceleration for the given measurement precision.

As aluminum flake-containing formulas readily detonated, it was determined that nanoscale spherical aluminum particles are not strictly necessary for mixtures of Al/water-H_2O_2 to sustain detonation. However, during material characterization, it was

determined that nanoscale features, such as flake thickness, are present in the flake powder. The relatively inexpensive flake powder represents a tool to further probe the aluminum-water system. Additionally, although not demonstrated to be detonable in this thesis, the capability of micron-scale aluminum to sustain detonation is not automatically precluded by the larger particle size.

The detonation is supported by reactions of aluminum particles with water on sub-microsecond timescales faster than previously thought possible. The exact mechanisms of this prompt aluminum reaction are yet to be elucidated. The fact that detonation can be supported by this truly binary reaction does not support the concept of heating the particles to a prescribed temperature before reaction occurs [4].

The detonation velocity results of the flake-Al trials were compared to Cheetah 2.0 thermochemical code calculations. The Cheetah results indicate a significant velocity deficit ($\sim$2 km s^{-1}) compared to the complete reaction. The source of this velocity deficit remains unclear.

Clearly a complex interplay exists between detonability, porosity, and peroxide concentration. The mechanism by which hydrogen peroxide sensitizes the aluminum-water mixtures to detonation is evidenced to be resultant from the production of oxygen-rich pores from hydrogen peroxide decomposition. Density plays an important role in the sensitivity of the Al/water-H_2O_2 in sustaining detonation. Although all mixtures tested had some degree of porosity, only an ideal range of mixture density sustained detonation.

It is possible the porosity provides the necessary hotspot features for sensitization. Additionally, detonation of mixtures was only observed in peroxide fractions of 10 wt% and above. Hydrogen peroxide is itself a detonable energetic monopropellant, and its inclusion may contribute to the sustained detonation, but is not sufficient on its own.

Chapter 7

Future Work

Further research is needed to fully explore the aluminum-water system. For the mixtures used in this study, the evolution of oxygen gas significantly alters the density of the mixture causing time-dependent inconsistencies in process parameters and large uncertainties in results. Large-volume single-batch process mixing may be used to create a uniform mixture. Investigation into void-sensitization of the aluminum-water system can be conducted through the introduction of GMBs, porous polystyrene, or gas-generating additives such as small fractions of calcium carbonate, to create well-defined, non-expanding mixtures.

Additionally, uncoated aluminum may be used. Coated particles were used in this study to suppress spontaneous reaction of the aluminum and water. Particle coating, although a small fraction of the charge (5 wt%), is not an inert component of the detonation reaction.

Thermochemical effects from the secondary components of hydrogen peroxide, Viton, and TRIM influence mixture detonability characteristics.

Rate stick investigations of formulations with consistent density are required to fully quantify the diameter effect. Charge diameters investigated in this research ranged from 38.1–93.8 mm, however charge contents were not consistent across formulation, density, or particle morphology. Flake-Al mixtures are ideal for rate stick investigations due to their ability to sustain detonation, and inexpensiveness for use in large-volume charges.

The mixtures currently presented in this work require materials and processing techniques generally inaccessible to the public. The high-test peroxide fractions used are regulated due to their use in peroxide-based explosives such as TATP. However, with optimization of the shot processing, detonability may be extended to mixtures of pure water and even larger aluminum particles, such as commercially accessible micron scale spherical powders. This issue is hence raised with the possibility of these commercially available ingredients being used in the formulation of homemade explosives.

Bibliography

[1] W. A. Trzciński and L. Maiz, "Thermobaric and enhanced blast explosives–properties and testing methods," *Propellants, Explosives, Pyrotechnics*, vol. 40, no. 5, pp. 632–644, 2015.

[2] L. Orth-Farrell and H. Krier, "Simulation of detonation in high explosives with aluminum particles," *Combustion Science and Technology*, vol. 161, no. 1, pp. 69–88, 2000.

[3] P. J. Haskins, M. D. Cook, and R. I. Briggs, "The effect of additives on the detonation characteristics of a liquid explosive," in *AIP Conference Proceedings*, vol. 620, pp. 890–893, American Institute of Physics, 2002.

[4] S. K. Chan, "Reaction delay of aluminum in condensed explosives," *Propellants, Explosives, Pyrotechnics*, vol. 39, no. 6, pp. 897–903, 2014.

[5] M. A. Cook, A. S. Filler, R. T. Keyes, W. S. Partridge, and W. Ursenbach, "Aluminized explosives," *The Journal of Physical Chemistry*, vol. 61, no. 2, pp. 189–196, 1957.

[6] B. C. Tappan, P. R. Bowden, V. W. Manner, J. A. Leiding, and M. S. Jakulewicz, "Evaluation of the deuterium isotope effect in the detonation of aluminum containing explosives," *Propellants, Explosives, Pyrotechnics*, vol. 43, no. 1, pp. 62–68, 2018.

[7] P. Brousseau and C. J. Anderson, "Nanometric aluminum in explosives," *Propellants, Explosives, Pyrotechnics*, vol. 27, no. 5, pp. 300–306, 2002.

[8] W. A. Trzciński, J. Paszula, and S. Grys, "Detonation and blast wave characteristics of nitromethane mixed with particles of an aluminium–magnesium alloy," *Propellants, Explosives, Pyrotechnics*, vol. 35, no. 2, pp. 85–92, 2010.

[9] J. Loiseau, S. Goroshin, D. L. Frost, A. J. Higgins, and F. Zhang, "Ability of metalized gelled nitromethane to accelerate a flyer plate," in *Proceedings of the Sixteenth International Detonation Symposium, Cambridge, MD*, 2018.

[10] Q. Pontalier, J. Loiseau, S. Goroshin, F. Zhang, and D. L. Frost, "Blast enhancement from metalized explosives," *Shock Waves*, vol. 31, no. 3, pp. 203–230, 2021.

[11] A. Maranda, "Research on the process of detonation of explosive mixtures of the oxidizer fuel type containing aluminium powder," *Propellants, Explosives, Pyrotechnics*, vol. 15, no. 4, pp. 161–165, 1990.

[12] D. Price, A. R. Clairmont, and J. O. Erkman, "Explosive behavior of aluminized ammonium perchlorate," *Combustion and Flame*, vol. 20, no. 3, pp. 389–400, 1973.

[13] T. R. Sippel, T. L. Pourpoint, and S. F. Son, "Combustion of nanoaluminum and water propellants: Effect of equivalence ratio and safety/aging characterization," *Propellants, Explosives, Pyrotechnics*, vol. 38, no. 1, pp. 56–66, 2013.

[14] M. W. Beckstead, "Correlating aluminum burning times," *Combustion, Explosion and Shock Waves*, vol. 41, no. 5, pp. 533–546, 2005.

[15] M. M. Schmitt, P. R. Bowden, B. C. Tappan, and D. Henneke, "Steady-state shock-driven reactions in mixtures of nano-sized aluminum and dilute hydrogen peroxide," *Journal of Energetic Materials*, vol. 36, no. 3, pp. 266–277, 2018.

[16] P. Julien, J. Vickery, S. Goroshin, D. L. Frost, and J. M. Bergthorson, "Freely-propagating flames in aluminum dust clouds," *Combustion and Flame*, vol. 162, no. 11, pp. 4241–4253, 2015.

[17] S. Goroshin, I. Fomenko, and J. Lee, "Burning velocities in fuel-rich aluminum dust clouds," *Symposium (International) on Combustion*, vol. 26, no. 2, pp. 1961–1967, 1996.

[18] J. Vickery, P. Julien, S. Goroshin, J. M. Bergthorson, and D. L. Frost, "Propagation of isobaric spherical flames in hybrid aluminum-methane fuel mixtures," *Journal of Loss Prevention in the Process Industries*, vol. 49, pp. 472–480, 2017.

[19] P. R. Amyotte, S. Chippett, and M. J. Pegg, "Effects of turbulence on dust explosions," *Progress in Energy and Combustion Science*, vol. 14, no. 4, pp. 293–310, 1988.

[20] M. Schoenitz, E. L. Dreizin, and E. Shtessel, "Constant volume explosions of aerosols of metallic mechanical alloys and powder blends," *Journal of Propulsion and Power*, vol. 19, no. 3, pp. 405–412, 2003.

[21] H. M. Cassel, *Some Fundamental Aspects of Dust Flames*. No. 2 in Report of investigations, U.S. Department of the Interior, Bureau of Mines, 1964.

[22] M. Soo, P. Julien, S. Goroshin, J. M. Bergthorson, and D. L. Frost, "Stabilized flames in hybrid aluminum-methane-air mixtures," *Proceedings of the Combustion Institute*, vol. 34, no. 2, pp. 2213–2220, 2013.

[23] M. Soo, S. Goroshin, N. Glumac, K. Kumashiro, J. Vickery, D. L. Frost, and J. M. Bergthorson, "Emission and laser absorption spectroscopy of flat flames in aluminum suspensions," *Combustion and Flame*, vol. 180, pp. 230–238, 2017.

[24] P. Julien, S. Whiteley, M. Soo, S. Goroshin, D. L. Frost, and J. M. Bergthorson, "Flame speed measurements in aluminum suspensions using a counterflow burner," *Proceedings of the Combustion Institute*, vol. 36, no. 2, pp. 2291–2298, 2017.

[25] M. McRae, P. Julien, S. Salvo, S. Goroshin, D. L. Frost, and J. M. Bergthorson, "Stabilized, flat iron flames on a hot counterflow burner," *Proceedings of the Combustion Institute*, vol. 37, no. 3, pp. 3185–3191, 2019.

[26] T. Bazyn, H. Krier, and N. Glumac, "Oxidizer and pressure effects on the combustion of 10-micron aluminum particles," *Journal of Propulsion and Power*, vol. 21, no. 4, pp. 577–582, 2005.

[27] P. Lynch, H. Krier, and N. Glumac, "A correlation for burn time of aluminum particles in the transition regime," *Proceedings of the Combustion Institute*, vol. 32, no. 2, pp. 1887–1893, 2009.

[28] T. Bazyn, H. Krier, and N. Glumac, "Combustion of nanoaluminum at elevated pressure and temperature behind reflected shock waves," *Combustion and Flame*, vol. 145, no. 4, pp. 703–713, 2006.

[29] N. Glumac, H. Krier, T. Bazyn, and R. Eyer, "Temperature measurements of aluminum particles burning in carbon dioxide," *Combustion Science and Technology*, vol. 177, no. 3, pp. 485–511, 2005.

[30] V. M. Boiko and S. V. Poplavski, "Self-ignition and ignition of aluminum powders in shock waves," *Shock Waves*, vol. 11, no. 4, pp. 289–295, 2002.

[31] T. Bazyn, H. Krier, and N. Glumac, "Evidence for the transition from the diffusion-limit in aluminum particle combustion," *Proceedings of the Combustion Institute*, vol. 31, no. 2, pp. 2021–2028, 2007.

[32] S. Goroshin, J. Mamen, A. Higgins, T. Bazyn, N. Glumac, and H. Krier, "Emission spectroscopy of flame fronts in aluminum suspensions," *Proceedings of the Combustion Institute*, vol. 31, no. 2, pp. 2011–2019, 2007.

[33] V. Tanguay, *Combustion of reactive metal particles in high-speed flow of detonation products*. PhD thesis, McGill University, Montreal, QC, 2009.

[34] D. A. Frank-Kamenetsky, *Diffusion and Heat Exchange in Chemical Kinetics*. Princeton University Press, 1955.

[35] L. A. Vulis, *Thermal regimes of combustion*. McGraw-Hill, 1961.

[36] M. Soo, S. Goroshin, J. M. Bergthorson, and D. L. Frost, "Reaction of a particle suspension in a rapidly-heated oxidizing gas," *Propellants, Explosives, Pyrotechnics*, vol. 40, no. 4, pp. 604–612, 2015.

[37] I. Glassman, "Combustion of metals: physical considerations," *ARS Progress in Astronautics and Rocketry: Solid Propellant Rocket Research*, vol. 1, pp. 253–257, 1960.

[38] N. N. Semenov, "Thermal theory of combustion and explosion," *Progress of Physical Science*, vol. 24, no. 4, 1942.

[39] M. Soo, X. Mi, S. Goroshin, A. J. Higgins, and J. M. Bergthorson, "Combustion of particles, agglomerates, and suspensions–a basic thermophysical analysis," *Combustion and Flame*, vol. 192, pp. 384–400, 2018.

[40] S. Whitaker, "Forced convection heat transfer correlations for flow in pipes, past flat plates, single cylinders, single spheres, and for flow in packed beds and tube bundles," *AIChE Journal*, vol. 18, no. 2, pp. 361–371, 1972.

[41] V. Tanguay, P. Batchelor, R. El-Saadi, and A. Higgins, "Metal combustion in high-speed flow," in *43rd AIAA Aerospace Sciences Meeting and Exhibit*, p. 361, 2005.

[42] V. Sarou-Kanian, J.-C. Rifflet, F. Millot, E. Véron, T. Sauvage, and I. Gökalp, "On the role of carbon dioxide in the combustion of aluminum droplets," *Combustion Science and Technology*, vol. 177, no. 12, pp. 2299–2326, 2005.

[43] P. Julien, M. Soo, S. Goroshin, D. L. Frost, J. M. Bergthorson, N. Glumac, and F. Zhang, "Combustion of aluminum suspensions in hydrocarbon flame products," *Journal of Propulsion and Power*, vol. 30, no. 4, pp. 1047–1054, 2014.

[44] A. J. Higgins, D. L. Frost, C. Knowlen, F. Zhang, and S. B. Murray, "Combustion of supersonic metallic spheres," in *18th International Colloquium on the Dynamics of Explosions and Reactive Systems, Seattle, WA*, 2001.

[45] P. Batchelor and A. J. Higgins, "Ignition of reactive metal particles in supersonic flow," in *Combustion Institute/Canadian Section Spring Technical Meeting, Kingston, Ontario*, 2004.

[46] A. Devito, P. Julien, S. Goroshin, and A. J. Higgins, "Investigation of supersonic combustion of bulk metal via spectroscopy," in *24th International Colloquium on the Dynamics of Explosions and Reactive Systems, Taipei, Taiwan*, 2013.

[47] J. H. S. Lee, *The Detonation Phenomenon.* Cambridge University Press, 2008.

[48] Y. B. Zel'dovich, "On the theory of the propagation of detonations on gaseous system," *Zhurnal Éksperimental'noĭ i Teoreticheskoĭ Fiziki*, vol. 10, no. 5, pp. 542–568, 1940.

[49] J. Von Neuman, "Theory of detonation waves," tech. rep., Institute for Advanced Study Princeton NJ, 1942.

[50] W. Döring, "Über den detonationsvorgang in gasen (On detonation processes in gases)," *Annalen der Physik*, vol. 435, no. 6-7, pp. 421–436, 1943.

[51] D. L. Chapman, "On the rate of explosion in gases," *The London, Edinburgh, and Dublin Philosophical Magazine and Journal of Science*, vol. 47, no. 284, pp. 90–104, 1899.

[52] É. Jouguet, "On the propagation of chemical reactions in gases," *Journal de Mathématiques Pures et Appliquées*, vol. 1, no. 347-425, p. 2, 1905.

[53] R. C. Ripley, *Acceleration and Heating of Metal Particles in Condensed Matter Detonation*. PhD thesis, University of Waterloo, Waterloo, ON, 2010.

[54] W. Davis and C. Fauquignon, "Classical Theory of Detonation," *Journal de Physique IV Proceedings*, vol. 05, no. C4, pp. C4–3–C4–21, 1995.

[55] P. W. Cooper, *Explosives engineering*. John Wiley & Sons, 2018.

[56] R. C. Ripley, F. Zhang, and F.-S. Lien, "Acceleration and heating of metal particles in condensed matter detonation," *Proceedings of the Royal Society A: Mathematical, Physical and Engineering Sciences*, vol. 468, no. 2142, pp. 1564–1590, 2012.

[57] Z. Y. Ding, M. A. Frisch, L. Li, and E. F. Gloyna, "Catalytic oxidation in supercritical water," *Industrial & engineering chemistry research*, vol. 35, no. 10, pp. 3257–3279, 1996.

[58] A. A. Vostrikov, O. N. Fedyaeva, I. I. Fadeeva, and M. Y. Sokol, "The formation of Al_2O_3 nanoparticles in the oxidation of aluminum by water under sub-and supercritical conditions," *Zhurnal Fizicheskoi Khimii B*, vol. 4, no. 7, pp. 1051–1060, 2010.

[59] K. A. Trowell, S. Goroshin, D. L. Frost, and J. M. Bergthorson, "The use of supercritical water for the catalyst-free oxidation of coarse aluminum for hydrogen production," *Sustainable Energy & Fuels*, vol. 4, no. 11, pp. 5628–5635, 2020.

[60] C. L. Mader, *Detonation properties of condensed explosives computed using the Becker-Kistiakowsky-Wilson equation of state*, vol. 2900. Los Alamos Scientific Lab., NM, 1963.

[61] E. Lee, M. Finger, and W. Collins, "JWL equation of state coefficients for high explosives," tech. rep., Lawrence Livermore National Lab., Livermore, CA, 1973.

[62] L. E. Fried, "Cheetah 1.0 users manual," tech. rep., Lawrence Livermore National Lab., CA, 1994.

[63] L. E. Fried, W. M. Howard, and P. C. Souers, "Kinetic modeling of non-ideal explosives with Cheetah," tech. rep., Lawrence Livermore National Lab., CA, 1998.

[64] F. P. Bowden and A. D. Yoffe, *Initiation and growth of explosion in liquids and solids*. CUP Archive, 1985.

[65] R. Engelke, "Effect of a physical inhomogeneity on steady-state detonation velocity," *The Physics of Fluids*, vol. 22, no. 9, pp. 1623–1630, 1979.

[66] R. Engelke, "Effect of the number density of heterogeneities on the critical diameter of condensed explosives," *The Physics of fluids*, vol. 26, no. 9, pp. 2420–2424, 1983.

[67] F. Zhang, P. A. Thibault, R. Link, and A. L. Gonor, "Momentum transfer during shock interaction with metal particles in condensed explosives," in *AIP Conference Proceedings*, vol. 620, pp. 934–937, American Institute of Physics, 2002.

[68] C. L. Mader, *The hydrodynamic hot spot and shock initiation of homogeneous explosives*, vol. 2703. Los Alamos Scientific Laboratory of the University of California, 1962.

[69] K. Yano, Y. Horie, and D. Greening, "A unifying framework for hot spots and ignition of energetic materials," tech. rep., Los Alamos National Lab., NM, 2001.

[70] W. C. Davis, "Introduction to detonation phenomena," tech. rep., Los Alamos Scientific Lab., NM, 1979.

[71] R. K. Kurbangalina, "Critical diameter of liquid explosives as a function of powder content," *Journal of Applied Mechanics and Technical Physics*, vol. 10, no. 4, pp. 656–659, 1969.

[72] A. M. Milne, "Detonation in heterogeneous mixtures of liquids and particles," *Shock Waves*, vol. 10, no. 5, pp. 351–362, 2000.

[73] C. L. Mader, "Numerical modeling of detonations," *Los Alamos Series in Basic and Applied Sciences*, 1979.

[74] C. L. Mader, J. D. Kershner, and G. H. Pimbley, "Three-dimensional modeling of inert metal-loaded explosives," *Journal of Energetic Materials*, vol. 1, no. 4, pp. 293–324, 1983.

[75] F. W. Sandstrom, R. L. Abernathy, M. G. Leone, and M. L. Banks, "Diameter effect and detonation front curvature of ideal and non-ideal explosives," in *AIP Conference Proceedings*, vol. 505, pp. 825–828, American Institute of Physics, 2000.

[76] D. L. Frost and F. Zhang, *Slurry Detonation*, pp. 169–216. Berlin, Heidelberg: Springer Berlin Heidelberg, 2009.

[77] L. Maiz and W. A. Trzciński, "A method to investigate the confined explosion of thermobaric and enhanced blast explosives," *American Journal of Engineering Research*, vol. 7, no. 4, pp. 139–147, 2018.

[78] Y. Kato and K. Murata, "Detonation characteristics of packed beds of metal particle saturated with nitromethane," in *21st International Colloquium on the Dynamics of Explosions and Reactive Systems*, 2007.

[79] Y. Kato, P. Bauer, C. Brochet, and R. Bouriannes, "Brightness temperature of detonation wave in nitromethane-tetranitromethane mixture and in gaseous mixtures at a high initial pressure," in *Proceedings of the Seventh International Detonation Symposium, Annapolis, MD*, pp. 768–774, 1981.

[80] A. P. Ershov, N. P. Satonkina, and G. M. Ivanov, "High-resolution conductivity profile measurements in detonating pressed explosive," *Technical Physics Letters*, vol. 30, no. 12, pp. 1048–1050, 2004.

[81] A. P. Ershov, N. P. Satonkina, and G. M. Ivanov, "Electroconductivity profiles in dense high explosives," *Zhurnal Fizicheskoi Khimii B*, vol. 1, no. 6, pp. 588–599, 2007.

[82] N. P. Satonkina, S. A. Bordzilovsky, D. A. Danilko, A. P. Ershov, S. M. Karakhanov, A. V. Plastinin, S. I. Rafeichik, and A. S. Yunoshev, "Influence of aluminum on the characteristics of detonating emulsion explosives," in *Journal of Physics: Conference Series*, vol. 1128, p. 012063, IOP Publishing, 2018.

[83] D. L. Frost, F. Zhang, S. B. Murray, and S. McCahan, "Critical conditions for ignition of metal particles in a condensed explosive," in *Proceedings of the Twelfth International Detonation Symposium, MD*, vol. 693, 2002.

[84] D. L. Frost, S. Goroshin, J. Levine, R. Ripley, and F. Zhang, "Critical conditions for ignition of aluminum particles in cylindrical explosive charges," in *AIP Conference Proceedings*, vol. 845, pp. 972–975, American Institute of Physics, 2006.

[85] D. L. Frost, S. Goroshin, R. Ripley, and F. Zhang, "Effect of scale on the blast wave from a metalized explosive," in *Proceedings of the Thirteenth International Detonation Symposium, MD*, vol. 97, 2006.

[86] V. Tanguay, A. J. Higgins, and F. Zhang, "A simple analytical model for reactive particle ignition in explosives," *Propellants, Explosives, Pyrotechnics*, vol. 32, no. 5, pp. 371–384, 2007.

[87] C. Capellos, E. L. Baker, S. Nicolich, W. Balas, J. Pincay, and L. I. Stiel, "Eigenvalue detonation of combined effects aluminized explosives," in *AIP Conference Proceedings*, vol. 955, pp. 357–360, American Institute of Physics, 2007.

[88] X. Li, H. Pei, X. Zhang, and X. Zheng, "Effect of aluminum particle size on the performance of aluminized explosives," *Propellants, Explosives, Pyrotechnics*, vol. 45, no. 5, pp. 807–813, 2020.

[89] A. Yoshinaka, F. Zhang, and W. Wilson, "Effect of shock compression on aluminum particles in condensed media," in *AIP Conference Proceedings*, vol. 955, pp. 1057–1060, American Institute of Physics, 2007.

[90] V. G. Ivanov, S. N. Leonov, G. L. Savinov, O. V. Gavrilyuk, and O. V. Glazkov, "Combustion of mixtures of ultradisperse aluminum and gel-like water," *Combustion, Explosion and Shock Waves*, vol. 30, no. 4, pp. 569–570, 1994.

[91] G. A. Risha, S. F. Son, R. A. Yetter, V. Yang, and B. C. Tappan, "Combustion of nano-aluminum and liquid water," *Proceedings of the Combustion Institute*, vol. 31, no. 2, pp. 2029–2036, 2007.

[92] J. L. Sabourin, G. A. Risha, R. A. Yetter, S. F. Son, and B. C. Tappan, "Combustion characteristics of nanoaluminum, liquid water, and hydrogen peroxide mixtures," *Combustion and Flame*, vol. 154, no. 3, pp. 587–600, 2008.

[93] A. G. Rozner and J. R. Holden, "Fast reactions of aluminum-a literature review," tech. rep., 1977.

[94] A. A. Shidlovskij, "Explosive mixtures of water and methanol with magnesium and aluminum," *Zhurnal Prikladnoi Khimii*, vol. 19, pp. 371–378, 1946.

[95] L. Medard, "On the explosive nature of mixtures of magnesium or aluminum with water or methanol," *Memorial des Poudres*, vol. 33, pp. 490–503, 1951.

[96] L. Medard, "The explosive character of hydrogen peroxide (le charactère explosif du bioxyde d'hydrogène)," *Comptes Rendus de l'Académie des Sciences*, vol. 9, no. 22, pp. 1941–1943, 1946.

[97] J. E. Parmeter, "Historical survey: German research on hydrogen peroxide/alcohol explosives," tech. rep., Sandia National Lab, Albuquerque, NM, 2015.

[98] T. Khmel, "Influence of the reaction of oxide decomposition on detonation structures in aluminum gas suspensions," in *AIP Conference Proceedings*, vol. 2027, p. 040013, AIP Publishing LLC, 2018.

[99] E. A. Tomic, "Chemical foaming and sensitizing of water-bearing explosives with hydrogen peroxide," Feb. 5 1974. US Patent 3,790,415.

[100] A. S. Yunoshev, V. V. Sil'Vestrov, A. V. Plastinin, and S. I. Rafeichik, "Influence of artificial pores on the detonation parameters of an emulsion explosive," *Combustion, Explosion, and Shock Waves*, vol. 53, no. 2, pp. 205–210, 2017.

[101] V. B. Storozhev and A. N. Yermakov, "Activation of aluminum nanopowder combustion in water vapor by O_2 additions," *Combustion and Flame*, vol. 200, pp. 82–84, 2019.

[102] C. Handley, B. Lambourn, N. Whitworth, H. James, and W. Belfield, "Understanding the shock and detonation response of high explosives at the continuum and meso scales," *Applied Physics Reviews*, vol. 5, no. 1, p. 011303, 2018.

[103] A. Campbell, W. Davis, and J. Travis, "Shock initiation of detonation in liquid explosives," *The Physics of Fluids*, vol. 4, no. 4, pp. 498–510, 1961.

[104] "Position Transducers." `http://dynasen.com/product-category/position-transducers/`. Accessed: 2021-08-23.

[105] J. Loiseau, *Validation of the Gurney Model for Heterogeneous Systems*. PhD thesis, McGill University, 2018.

[106] J. A. Puszynski, C. J. Bulian, and J. J. Swiatkiewicz, "Processing and ignition characteristics of aluminum-bismuth trioxide nanothermite system," *Journal of Propulsion and Power*, vol. 23, no. 4, pp. 698–706, 2007.

[107] A. Hiroki and J. A. LaVerne, "Decomposition of hydrogen peroxide at water- ceramic oxide interfaces," *The Journal of Physical Chemistry B*, vol. 109, no. 8, pp. 3364–3370, 2005.

[108] S. I. Jackson, "An analytic method for two-dimensional wall motion and product isentrope from the detonation cylinder test," *Proceedings of the Combustion Institute*, vol. 35, no. 2, pp. 1997–2004, 2015.

[109] S. I. Jackson, "The dependence of ammonium-nitrate fuel-oil (ANFO) detonation on confinement," *Proceedings of the Combustion Institute*, vol. 36, no. 2, pp. 2791–2798, 2017.

[110] L. L. Davis and L. G. Hill, "ANFO cylinder tests," in *AIP conference proceedings*, vol. 620, pp. 165–168, American Institute of Physics, 2002.

[111] E. A. Gulbransen and W. S. Wysong, "Thin oxide films on aluminum," *The Journal of Physical Chemistry*, vol. 51, no. 5, pp. 1087–1103, 1947.

[112] B. M. Dobratz and P. C. Crawford, *LLNL explosives handbook: properties of chemical explosives and explosive simulants*. University of California, 1985.

[113] D. H. Bross and B. Ruscic, "ATcT enthalpies of formation based on version 1.122p of the Thermochemical Network." `https://atct.anl.gov/Thermochemical%20Data/version%201.122/species/?species_number=847`. Accessed: 2021-07-31.

[114] J. P. Coughlin and G. J. Warren, "Heat of Formation of Viton A by Combustion Calorimetry," *Journal of Chemical and Engineering Data*, vol. 6, no. 1, pp. 14–15, 1961.

Appendix A

Cheetah-Calculated Properties

This section provides an example of Cheetah-calculated properties and JWL expansion coefficients of the Al/water-H_2O_2 system for varying fractions of reacting aluminum. The Cheetah input code detailing mass fractions of each mixture component may be generated using the MATLAB code provided in Appendix B. JWL coefficients are for the JWL form [112]:

$$P_{\mathrm{JWL}} = A \exp\left(-R_1 \frac{\nu}{\nu_0}\right) + B \exp\left(-R_2 \frac{\nu}{\nu_0}\right) + \frac{C}{(\nu/\nu_0)^{1+w}}$$

The following mixture components were added to the Cheetah input file `formula.in` [113, 114]. Heat of formation of TRIM was estimated using bond enthalpies:

```
form, hydrogen peroxide, 1.450000, -187.341000, h, 2, o, 2
form, trim, 1.060000, -998.380000,    c, 18, h, 26, o, 6
form, viton, 1.850000, -1392.000000,  c, 5,  h, 3.5, f, 6.5
```

	Al_{react}	P_{CJ}, GPa	ρ_{CJ}, g cm^{-3}	E, kJ cm^{-3}	T, K	D_{CJ}, mm µs^{-1}	u_{CJ}, mm µs^{-1}	c_{CJ}, mm µs^{-1}	γ	E_{tot}, kJ cm^{-3}	A	B	C	R_1	R_2	ω
Nano-Al	0.20	1.29	1.273	0.16	1036	2.320	0.581	1.739	2.992	-0.844	-	-	-	-	-	-
	0.30	1.78	1.256	0.21	1412	2.787	0.670	2.117	3.157	-1.498	98.22	0.55	0.32	5.93	1.02	0.21
	0.40	2.34	1.257	0.28	1814	3.191	0.770	2.421	3.144	-2.152	77.02	0.31	0.28	4.92	0.51	0.10
	0.50	3.20	1.328	0.45	2147	3.448	0.972	2.476	2.547	-2.746	56.48	0.58	0.44	4.50	0.81	0.17
	0.60	3.24	1.267	0.40	2417	3.708	0.916	2.792	3.048	-3.366	165.39	1.60	0.54	5.95	1.14	0.18
	0.70	3.73	1.265	0.46	2731	3.985	0.981	3.004	3.063	-3.938	182.45	1.53	0.60	5.83	1.00	0.17
	0.80	4.24	1.264	0.52	3053	4.256	1.043	3.213	3.079	-4.554	194.02	1.57	0.68	5.69	0.97	0.17
	0.90	4.91	1.274	0.62	3404	4.526	1.136	3.390	2.984	-5.207	119.74	0.63	0.76	4.59	0.65	0.17
	1.00	6.63	1.348	0.97	3871	4.878	1.426	3.452	2.421	-5.869	84.62	0.45	0.83	3.94	0.59	0.16
Flake-Al	0.20	1.29	1.253	0.16	1155	2.366	0.573	1.794	3.132	-1.154	69.42	0.35	0.25	5.92	0.98	0.20
	0.30	1.85	1.261	0.23	1661	2.810	0.694	2.116	3.051	-1.940	75.06	0.35	0.34	5.49	0.90	0.17
	0.40	2.41	1.261	0.30	2097	3.203	0.791	2.411	3.047	-2.603	108.10	0.83	0.39	5.68	1.00	0.15
	0.50	2.74	1.272	0.35	2351	3.373	0.855	2.519	2.947	-3.258	102.92	1.16	0.47	5.51	1.01	0.15
	0.60	3.21	1.269	0.40	2690	3.664	0.922	2.742	2.972	-3.843	217.57	1.82	0.44	6.48	0.94	0.10
	0.70	3.70	1.266	0.46	3035	3.948	0.986	2.962	3.003	-4.470	103.22	0.73	0.54	4.81	0.61	0.11
	0.80	5.21	1.350	0.77	3484	4.303	1.276	3.027	2.373	-5.174	68.91	0.50	0.76	4.14	0.60	0.17
	0.90	7.01	1.414	1.15	3981	4.740	1.557	3.183	2.044	-5.921	56.90	0.14	0.86	3.51	0.40	0.16
	1.00	7.33	1.422	1.22	4075	4.818	1.601	3.218	2.010	-6.682	56.46	2.97	0.93	3.67	1.54	0.16

Table A.1: Al/Water-10 wt% H_2O_2 detonation properties and JWL coefficients from Cheetah 2.0, BKWC library. Initial density $\rho_0 = 0.95\,\mathrm{g/cm^3}$.

Appendix B

Cheetah Input MATLAB Code

This section provides a MATLAB script to easily create an input file `cheetahinput.txt` for Cheetah 2.0 to calculate estimated detonation properties of the Al/water-H_2O_2 system with varying bulk mixture density, peroxide fraction, and assigned fraction of reacting aluminum.

```
close all; clear all; clc;

HP  = [0      1.91   5.99   9.23   13.47  17.44  21.44 ];
dHP = [0.9970 1.0036 1.0179 1.0295 1.0452 1.0597 1.0737];
[a,~] = polyfit(HP,dHP,1);

fid = fopen('cheetahinput.txt','wt');

rho_Al = 2.70;
```

```
10 rho_Al2O3 = 3.95;
11 rho_TRIM = 1.06;
12 rho_O2 = 0.001429;
13 rho_viton = 1.85;
14
15 Al = 0; % 0 for flake, 1 for V-ALEX
16
17 for HPo = [10 15 20] % hydrogen peroxide fractions
18     rho_HPo = polyval(a,HPo);
19     for al_react = [0.2:0.1:1] % fraction of reacting Al
20         for rho = [0.7:0.025:1.2] % density range evaluated
21
22             if Al = 0 % flake Al
23                 x = (1/rho - 0.4489/rho_Al - 0.0512/rho_TRIM - 0.5/rho_HPo
                       )/(1/0.001429-1/rho_HPo);
24                 s1 = ['composition, al, ',num2str(44.89*al_react),', al
                       inert, ',num2str(44.89*(1-al_react)),', trim, 5.12,
                       oxygen, ',num2str(100*x),', hydrogen peroxide, ',
                       num2str((HPo*0.5-100*x)),', water, ',num2str((0.5*(100-
                       HPo))),', weight'];
25
26             elseif Al = 1 % V-ALEX
27                 x = (1/rho - 0.39090909/rho_Al - 0.027273/rho_Al2O3 -
                       0.040909/rho_viton - 90/165/rho_HPo)/(1/0.001429-1/
```

```
                    rho_HPo);
28                  s1 = ['composition, al, ',num2str(al_react*86*75/165),',
                    al inert, ',num2str((1-al_react)*86*75/165),', al2o3, '
                    , num2str(6*75/165),', viton, ',num2str(9*75/165),',
                    oxygen, ',num2str(100*x),', hydrogen peroxide, ',
                    num2str((HPo*9/16.5-100*x)),', water, ',num2str
                    ((90/165*(100-HPo))),', weight'];
29              end
30
31              % optional Cheetah commands
32              %s2 = ('fix concentration, al2o3-solid, 0, mole');
33              %s3 = ('fix concentration, al2o3-liquid, 0, mole');
34
35              s4 = ('standard run, TMD, 100');
36
37              %fprintf(fid, '%s\n%s\n%s\n%s\n', s1, s2, s3, s4);
38              fprintf(fid, '%s\n%s\n', s1, s4);
39          end
40      end
41  end
42  fclose(fid);
```

Appendix C

Analytic P-ν Behaviour from Wall Motion for Slab Geometry

This section provides a brief derivation for the 2D slab geometry case of the analytic method for two-dimensional wall motion and product P-ν behaviour, adapted from the original work by Jackson [108,109]. For explanation of all symbols used in the derivation, and details concerning the radially-symmetric case for cylinder test data, please refer to the original work by Jackson. The following section may be useful for future analysis of slab geometry test data of the aluminum-water system.

C.1 Pressure, P

This section derives, using Newton's second law of motion, a formula for product pressure P in terms of wall material density ρ_w, wall thickness t_w, internal wall angle θ_i, external pressure P_e, and PDV-measured outer wall acceleration $\frac{\mathrm{d}v_o}{\mathrm{d}t}$.

$$F_{p,v_o} = m\frac{\mathrm{d}v_o}{\mathrm{d}t}$$

$$F_{p,v_o} = F_p\cos(\theta_i)$$

$$F_p = w\mathrm{d}\ell P$$

$$m = \rho_w t_w w\mathrm{d}\ell$$

$$\mathrm{d}\ell P\cos(\theta_i) = \rho_w t_w \mathrm{d}\ell\frac{\mathrm{d}v_o}{\mathrm{d}t}$$

$$\boxed{P = \frac{\rho_w t_w}{\cos(\theta_i)}\frac{\mathrm{d}v_o}{\mathrm{d}t} + P_e}$$

C.2 Specific Volume of the Products, ν_p

This section derives a formula for specific volume of the products ν_p in terms of product thickness t_i, explosive initial density ρ_e, detonation velocity D, explosive initial thickness T_i, product pressure P, internal wall angle θ_i, and external pressure P_e.

Flow continuity:

$$u_p(t,x) = \frac{V_p(x)}{\sqrt{1 + t^2\left(\frac{\tan(\theta_i)}{t_i}\right)^2}}$$

Conservation of mass:

$$\rho_e DT_i = \rho_p \int_0^{t_i} u_p(t,x)\mathrm{d}t$$

Continuity into conservation of mass:

$$\rho_e DT_i = \rho_p V_p(x) \int_0^{t_i} \frac{1}{\sqrt{1+t^2\left(\frac{\tan(\theta_i)}{t_i}\right)^2}}\mathrm{d}t$$

$$\int \frac{1}{\sqrt{1+t^2x^2}}\mathrm{d}t = \frac{\sinh^{-1}(tx)}{x} + C, \qquad x = \frac{\tan(\theta_i)}{t_i}$$

$$\left[t_i \frac{\sinh^{-1}\left(t\frac{\tan(\theta_i)}{t_i}\right)}{\tan(\theta_i)}\right]_{t=0}^{t=t_i} = \left[t_i \frac{\sinh^{-1}(\tan(\theta_i))}{\tan(\theta_i)}\right] - [0]$$

$$\rho_e DT_i = \rho_p V_p(x) \left[t_i \frac{\sinh^{-1}(\tan(\theta_i))}{\tan(\theta_i)}\right]$$

$$V_p(x) = \frac{\rho_e DT_i \tan(\theta_i)}{t_i \rho_p \sinh^{-1}(\tan(\theta_i))}$$

Conservation of momentum:

$$\rho_p \int_0^{t_i} u_p(t,x)^2\mathrm{d}t = \rho_e D^2 T_i - Pt_i + F_\mathrm{b} + P_e T_i = \mathrm{RHS}$$

$$\rho_p V_p(x)^2 \int_0^{t_i} \frac{1}{1+t^2\left(\frac{\tan(\theta_i)}{t_i}\right)^2}\mathrm{d}t = \mathrm{RHS}$$

$$\int \frac{1}{1+t^2x^2}\mathrm{d}t = \frac{\tan^{-1}(tx)}{x} + C, \qquad x = \frac{\tan(\theta_i)}{t_i}$$

$$\left[t_i \frac{\tan^{-1}\left(t\frac{\tan(\theta_i)}{t_i}\right)}{\tan(\theta_i)}\right]_{t=0}^{t=t_i} = \left[t_i \frac{\tan^{-1}\left(\tan(\theta_i)\right)}{\tan(\theta_i)}\right] - [0]$$

$$\rho_p V_p(x)^2 \left[t_i \frac{\tan^{-1}\left(\tan(\theta_i)\right)}{\tan(\theta_i)}\right] = \mathrm{RHS}$$

Eliminate $V_p(x)$:

$$\rho_p \left[\frac{\rho_e D T_i \tan(\theta_i)}{t_i \rho_p \sinh^{-1}\left(\tan(\theta_i)\right)}\right]^2 \left[t_i \frac{\tan^{-1}\left(\tan(\theta_i)\right)}{\tan(\theta_i)}\right] = \mathrm{RHS}$$

$$\nu_p \frac{\tan(\theta_i)\tan^{-1}\left(\tan(\theta_i)\right)}{\sinh^{-1}\left(\tan(\theta_i)\right)^2} \frac{\rho_e^2 D^2 T_i^2}{t_i} = \mathrm{RHS}$$

$$\boxed{\nu_p = A\frac{t_i}{\rho_e^2 D^2 T_i^2}\left(\rho_e D^2 T_i - P t_i + F_\mathrm{b} + P_e T_i\right)}$$

$$\boxed{F_\mathrm{b} = \int_0^x P(x)\tan(\theta_i)\mathrm{d}x \approx 0}$$

$$\boxed{A = \frac{\sinh^{-1}\left(\tan(\theta_i)\right)^2}{\tan(\theta_i)\tan^{-1}\left(\tan(\theta_i)\right)} \approx 1}$$